ORIGINAL ARTICLE

lajss.org Latin American Journal of Solids and Structures

www.lajss.org

Innovated shear deformable FE formulations for the analyses of steel beams strengthened with orthotropic GFRP laminates

Thanh Bui-Tien[a], Phe Van Pham[a]*

[a]Faculty of Civil Engineering, University of Transport and Communications, #3 Cau Giay, Hanoi, Vietnam. Email: btthanh@utc.edu.vn, phe.phamvan@utc.edu.vn

* Corresponding author

https://doi.org/10.1590/1679-78257549

Abstract

The present study develops an innovated shear deformable theory and four finite element formulations based on a total potential energy variational principle for the analysis of steel beams strengthened with GFRP laminates. The present theory captures orthotropic properties of the GFRP laminae, GFRP lamina stacking sequences, partial interaction between the steel beam and the GFRP laminates, and shear deformations. Three examples are conducted for the validation of the present theory. Through comparisons, the system responses predicted by the present solutions are excellently validated against those of recent experimental studies and three-dimensional finite element analyses. Key results obtained in the present study include: (i) the responses of GFRP-strengthened beams are strongly influenced by GFRP fiber angle arrangements. (ii) The strengthening is the most effective for steel beams strengthened with a GFRP laminate stacked with fiber angles of 0 degree. Based on two parametric studies, the effects of the orthotropic GFRP lamina properties and GFRP laminate thicknesses on the system deflections are also investigated.

Keywords

Static response, orthotropic laminate, GFRP strengthening, continuous steel beam, finite element formulation.

Graphical Abstract

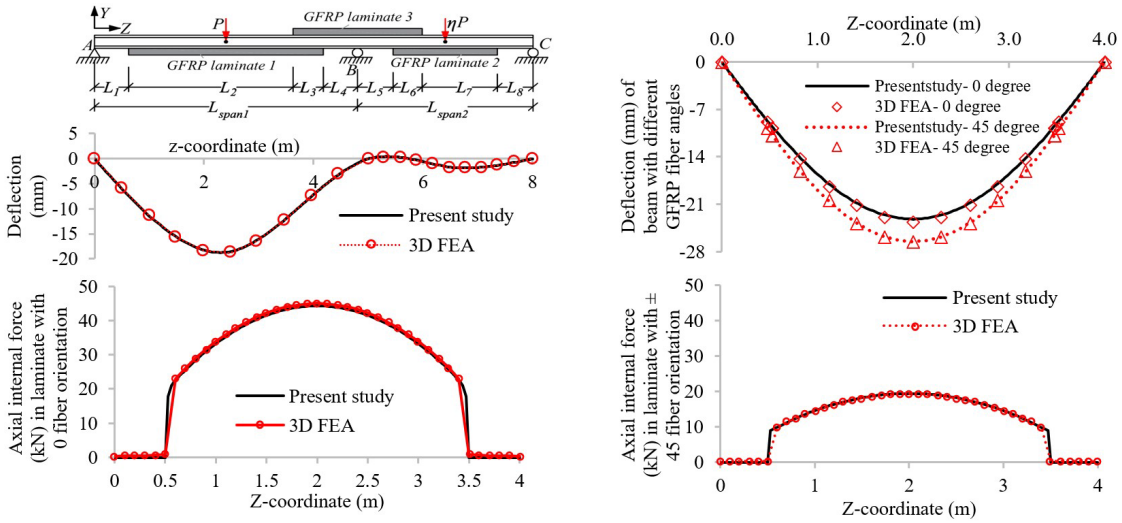

Received: March 03, 2023. In revised form: April 15, 2023. Accepted: April 19, 2023. Available online: April 27, 2023.
https://doi.org/10.1590/1679-78257549

1 Literature review

1.1 Introduction

Single or multiple span steel beams with wide flange cross-sections have been widely installed as main load carrying members in bridges, buildings, and other civil structures. However, load capacities of such old beams may be decreased because of corrosion and degradation (El Damatty and Abushagur 2003, El Damatty et al. 2003). Also, there maybe demands to increase the capacities of such existing beams so that they can carry higher load levels. In such cases, a beam strengthening solution may be required. However, traditional strengthening solutions by using bolds or welds to tightly attach strengthening plates to the steel surfaces may meet difficulties in installation. Recently, Glass Fiber Reinforced Polymer (GFRP) laminates have been widely being studied as an effective strengthening solution for steel members (El Damatty and Abushagur 2003, El Damatty et al. 2003, Harries and El-Tawil 2008, Parvathi et al. 2018). GFRP laminates are light, and they can be easily and fast installed to the steel surfaces by using adhesives. Also, they can be economically manufactured into relatively thick plates capable of resisting tensile, compression and shear stresses (El Damatty and Abushagur 2003, El Damatty et al. 2003, Correia et al. 2011, Ali et al. 2021). El Damatty et al. (2003) conducted an experimental study for wide flange steel beams strengthened with GFRP laminates bonded on to the top and bottom beam flanges, the study reported the increases of 23% for the yielding moment and 78% for the ultimate capacity of the system. GFRP laminates bonded to the compression flanges of steel beams may also help to increase local and global buckling resistances for the systems (El Damatty and Abushagur 2003, El Damatty et al. 2003, Correia et al. 2011). Similar effectiveness was also reported in other studies of steel members strengthened with GFRP laminates (e.g., Aguilera and Fam 2013, Aydin and Aktas 2015, Raj et al. 2016, Hosseini et al. 2021, Lesani et al. 2022).

Although there are such potential applications of GFRP laminates for the strengthening of steel beam, the mechanical behaviors in the GFRP-strengthened steel beams under transverse loadings are relatively complicative. Because GFRP laminates are typical composite materials, in which their stiffnesses are strongly depended on orthotropic GFRP laminae and lamina stacking sequences with different fiber orientation angles (Parvathi et al. 2018, Correia et al. 2011, Lee and Lee 2004). Besides, a GFRP laminate is often bonded to a steel member by using a thin adhesive layer with an elasticity modulus considerably lower than those of steel and GFRP materials, this may lead to a partial interaction between the steel member and the GFRP laminate (i.e., a plane composite cross-section doesn't remain plane after deformation) (El Damatty et al. 2003). Also, shear deformations in steel beams and GFRP laminates may influence on the deformations of such composite systems (Lee and Lee 2004, Phe and Mohareb 2014). As a result, the stresses and deformations in the GFRP-strengthened steel beams will be significantly influenced by the above discussed behaviors. To accurately capture such stresses and deformations, three-dimensional finite element solutions based on commercial finite element analysis packages may be developed. However, such solutions often involve in expensive computation costs and consume time for model treatments and result extractions. Therefore, it is necessary to develop simple beam solutions those have a low computation cost and a fast-running time, and they can accurately predict the responses of the GFRP-strengthened steel beams (as accurately as commercial finite element analyses do). Such simple solutions may also facilitate parametric studies to find out reasonable design configurations for the GFRP-strengthened steel beams.

1.2 Typical theories developed for the stress and deformation predictions of composite structures

There are numerous theories developed for the analysis of stresses and deformations of general composite structures. Lee and Lee (2004) and Back and Will (2008) developed finite element formulations based on Lagrange and Hermitian interpolation functions for the analysis of laminated composite beams. Ditaranto (1973) and Nowzartash and Mohareb (2005) developed analytical solutions for the static analyses of sandwich beams with a soft core. Koutsawa and Daya (2007) developed numerical and analytical solutions for analyses of laminate glass members attached by thin adhesive layers. Maddur and Chaturvedi (1999) developed a shear deformation theory for analysis of laminated composite open sections. Asta (2001) developed a composite beam theory for the analysis of two-layer composite beams with a weak shear connection at the interface. Gara et al. (2006) and Girhammar and Pan (2007) developed analytical solutions for the static analyses of two-layer composite beams with partial interactions between layers, in which the partial interactions were modeled by springs. Smith and Teng (2001) developed beam theories for the stress analyses of reinforced concrete beams strengthened with FRP plates. Ranzi and Zona (2007) developed a steel-concrete composite model with partial interactions at the interface. Challamel et al. (2010) and Challamel and Girhammar (2012) developed numerical and analytical solutions for the out-of-plane analyses of composite beams with interlayer slips. Recently, Sun et al. (2022) presented a numerically stable exact method for the analysis of partial-interaction composite beams based on Timoshenko beam theory. Andrade et al (2023) developed a linear 2D model for the analyses of two-layer plates with partial shear interaction. Although there have been many theories thus developed for the analyses of composite structures, they almost targeted at specified members those are different to composite systems of wide flange steel beams bonded with orthotropic GFRP laminates by using adhesive layers.

1.3 Typical numerical and analytical studies for the analyses of GFRP-strengthened steel beams

There have been many experiment studies conducted for strengthening of steel members by using GFRP laminates (e.g., El Damatty and Abushagur 2003, El Damatty et al. 2003, Aguilera and Fam 2013, Aydin and Aktas 2015, Parvathi et al. 2018, Correia et al. 2011). However, the numerical and analytical studies for such structures have not been widely and fully studied. El Damatty and Abushagur (2003) presented an analytical solution to predict the responses of the adhesive stresses/strains in GFRP-strengthened steel members. The adhesive layer was considered as elastic springs to connect GFRP laminates to steel member. The orthotropic GFRP lamina properties and lamina stacking sequences of GFRP laminates were not considered in their study. El Damatty et al. (2003) developed a numerical solution based on a commercial finite element program (ANSYS) for the stresses and deformations analyses of W150x35 beams strengthened with GFRP plates by bonding. In their model, the adhesive layers were replaced by elastic springs with zero thicknesses while the steel beams and GFRP laminates were modeled by brick elements. Accord and Earls (2006) conducted a numerical study to investigate the ductility of steel beams strengthened with GFRP laminates bonded to the compression beam flanges. The numerical model was developed in a commercial software package ADINA, in which the wide flange steel beam was modelled by using 4-node shell elements while the adhesive layers and GFRP plates were modelled by using 8-node brick elements. Youssef (2006) developed an analytical solution for the prediction of linear and nonlinear behaviors of steel beams strengthened with GFRP laminates. However, his solution was only applicable to simply supported beams. Siddique and El Damatty (2012, 2013) presented numerical studies to evaluate the improvement of buckling capacities of steel beams strengthened with GFRP laminates bonded to both top and bottom flanges. The numerical studies were conducted by using a finite element model in which the adhesive layer was again modeled as elastic springs with zero thicknesses while the steel and GFRP were modeled as 13-node shell elements developed by Koziey and Mirza (1997). Such finite element models were then adopted in a numerical study to investigate the factors of overstrength and ductility for moments in steel frames strengthened with GFRP laminates. The finite element model treatments based on the above discussed studies have some difficulties to apply to predict the responses of GFRP-strengthened steel beams, because they require to evaluate equivalent spring stiffnesses those replace the role of the adhesive layers. Also, they did not consider the effects of orthotropic GFRP lamina properties and lamina stacking sequences on the GFRP laminate stiffnesses. Phe and Mohareb (2014, 2015), Phe et al. (2017, 2018), Phe (2021) developed shear and non-shear deformable theories for the static and buckling analyses of steel beams strengthened with isotropic GFRP laminates bonded to the tension beam flanges. Zaghian and Mohareb (2019) developed a finite element formulation for the elastic buckling analysis of steel plates symmetrically strengthened with GFRP plates, in which GFRP plates were assumed as an isotropic material.

A general observation from the above discussed studies is that the GFRP laminates in GFRP-strengthened beams were treated as isotropic materials. However, they are hardly isotropic, and they are typically pultruded by orthotropic laminae stacked with different fiber orientation angles (e.g., 0^0, 45^0, or 90^0). Thus, axial and flexural stiffnesses of the GFRP laminates are accordingly influenced (Correia et al. 2011), Parvathi et al. 2018, Ibrahim et al. 2018, Phe 2022) and such effects have not been investigated yet. Besides, as GFRP laminates are often bonded to the steel flanges by using low modulus adhesive materials, those may create partial interactions between the steel flanges and the GFRP laminates. To model such a behavior, past numerical solutions used various spring, shell, and brick elements available in commercial finite element analyses packages (e.g., El Damatty et al. 2003, Siddique and El Damatty 2012) or simplified closed form solutions and finite element formulations based on beam theories (e.g., Youssef 2006, Phe 2021, Zaghian and Mohareb 2019). However, such numerical models are inapplicable for the steel beams strengthened with orthotropic GFRP laminates under various loading and boundary conditions. Within this context, the present study is going to fill in the gap by developing an innovated shear deformable theory and a group of simple finite element formulations for the stresses and deformations analyses of single or multiple span steel beams strengthened with orthotropic GFRP laminates bonded to the top and/or bottom beam flanges under various loading and boundary conditions. The theory captures the orthotropic GFRP lamina properties and GFRP lamina stacking sequences, partial interaction between the steel beam and the GFRP laminate, and shear deformations due to transverse bending. Among various possible failure modes of GFRP-strengthened steel beams (e.g., moment resistance based on steel yielding, that based on steel plastification, deflections, GFRP rupture strength, adhesive shear and peeling failures, fatigue, local/global buckling), the present study is applicable to the check of failure modes based on moment resistance based on steel yielding, GFRP stress control, deflection, pre-buckling analysis.

2 Description of the problem

Single- or multiple-span prismatic steel beams strengthened with orthotropic GFRP laminates are considered. An element of the steel beam strengthened with two GFRP laminates bonded to the top and bottom steel flanges by using adhesive layers is given in Figure 1a,b. Three other elements of the steel beam, of which the flanges are strengthened

with a top GFRP laminate (Figure 1c), a bottom GFRP laminate (Figure 1d), or not strengthened (Figure 1e), are also considered. The steel element strengthened with two GFRP laminates is considered as a general case. The steel beam has basic cross-section dimensions h, b, t_f, and t_w (Figure 1e). The thickness of GFRP laminate 1 is t_{g1}, while that of the adhesive layer 1 is t_{a1}, that of the GFRP laminate 2 is t_{g2}, and that of the adhesive layer 2 is t_{a2} (Figure 1c,d). The beam is assumed to subject point loads P_y and distributed loads q_y. Material definitions of steel, adhesive, and GFRP are given in Section 3.4 of the present study. It is required to develop a shear deformable theory and finite element formulations for the stress and deformation analyses of the given GFRP-strengthened steel beams.

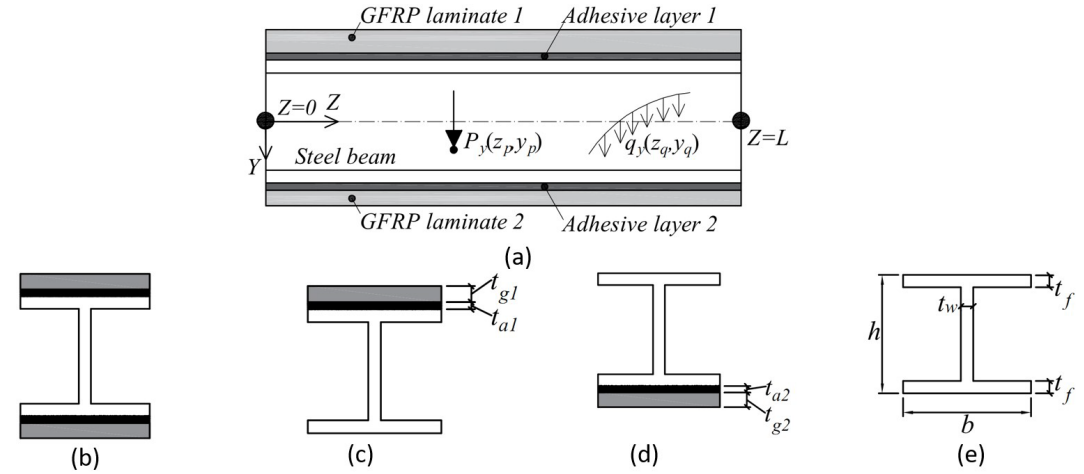

Figure 1 Statement of the problem: (a) A general element of a steel beam bonded with two GFRP laminates; and the cross-sections of four steel beam elements (b) bonded with top and bottom GFRP laminates, (c) bonded with a top GFRP laminate, (d) bonded with a bottom GFRP laminate, and (e) not strengthened.

3 Development of the general finite element formulations

3.1 Kinematic assumptions and governing displacements

In order to develop the present theory, the following kinematic assumptions are made: (i) Shear deformations due to transverse bending are captured in the steel beam and the GFRP laminates, (ii) Interaction between the steel member and the GFRP laminates are partial, in which displacements in the adhesive layer are linearly interpolated from those of the steel and the laminates.

Figure 2 presents a part of plan view of a GFRP-strengthened steel beam before and after deformation. The cross-section of the strengthened beam is initially plane before deformation, but it doesn't remain plane after deformation due to the weak behavior of the adhesive layers. Five governing displacements $W_1(z)$, $W_2(z)$ $W(z)$, $V(z)$ and $\theta_x(z)$ are proposed to describe such a deformation, in which $W_1(z)$ is the longitudinal displacement field of centroid O_{g1} of the GFRP laminate 1 cross-section, $W_2(z)$ is that of centroid O_{g2} of the GFRP laminate 2 cross-section, $W(z)$ is that of centroid O of the non-strengthened steel beam cross-section, $V(z)$ is the transverse displacement field and $\theta_x(z)$ is the transverse bending angle field of all materials, where $\theta_x(z)$ may be different to $\partial V(z)/dz$.

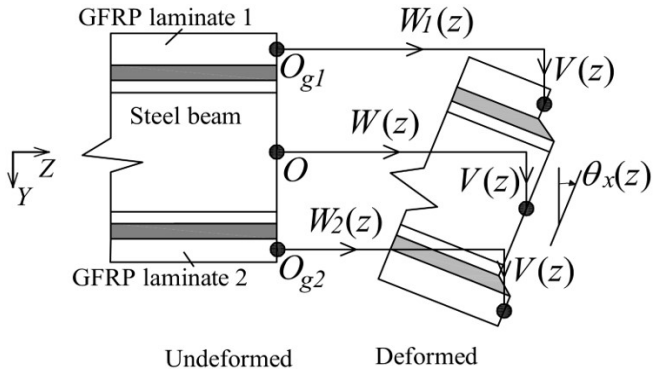

Figure 2 Governing displacement fields of the steel beams and GFRP laminates (a part of elevation view)

3.2 Develop through-thickness displacements

Through-thickness displacements in the steel beam:

To capture partial interactions between materials, a global coordinate system $OXYZ$ is assigned for the steel section while local coordinates $Cs_s n_s z$ are assigned to the thickness contours of the steel (Figure 3a). In which origins C lies on the contours of the steel section, s_s is the curvilinear contour coordinate measured from Origin 0, n_s is the normal-to-tangent axis of the contour measured from the contour, and z is the longitudinal axis. The through-thickness displacement fields at a Point with coordinates (s_s, n_s, z) are depicted as u_s, v_s, w_s (Figure 3b).

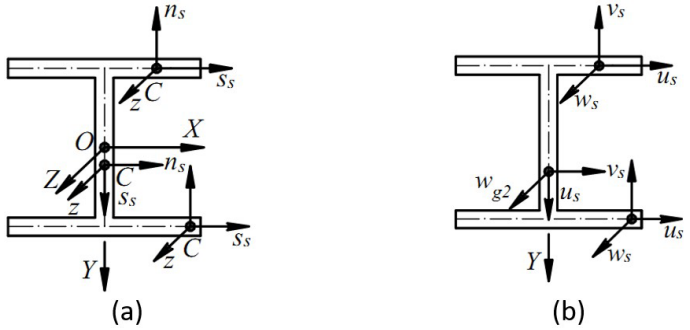

Figure 3 Definitions of (a) Local coordinate systems and (b) through-thickness displacement fields in the steel cross-section

Displacement fields u_s, v_s, w_s can be assumed in terms of the governing displacement fields as

$$\begin{aligned} u_s(s_s, n_s, z) &= \sin\alpha(s_s) V(z), \\ v_s(s_s, n_s, z) &= -\cos\alpha(s_s) V(z), \\ w_s(s_s, n_s, z) &= W(z) + n_s \cos\alpha(s_s) V'(z) - y(s_s)\theta_x(z) \end{aligned} \tag{1}$$

in which $\alpha(s_s)$ is an angle between the positive directions of the s_s-axis and X-axis (Figure 3a) and it is taken positive in the clockwise direction from the X-axis.

Through-thickness displacements in the GFRP laminates 1 and 2:

A global coordinate system $O_{g1}XY_{g1}Z$ and a local coordinate $C_{g1}s_{g1}n_{g1}z$ are assigned for the GFRP laminate 1 cross-section (Figure 4a). The meaning of the coordinate definitions are similar to those of the steel. The through-thickness displacement fields at a Point with coordinates (s_{g1}, n_{g1}, z) are depicted as u_{g1}, v_{g1}, w_{g1} (Figure 4b), where u_{g1} = 0 because the present laminate only consider longitudinal-transverse responses.

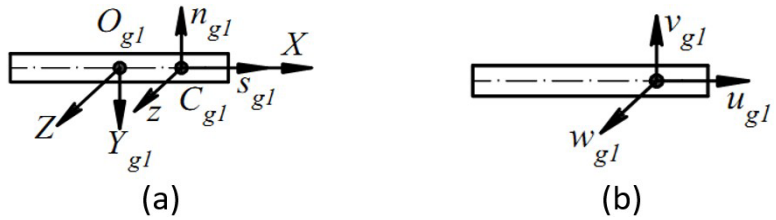

Figure 4 Definitions of (a) Local coordinate system and (b) through-thickness displacement fields in the GFRP laminate 1 section

Displacement fields v_{g1}, w_{g1} can be assumed in terms of the governing displacement fields as

$$v_{g1}(s_{g1}, n_{g1}, z) = -V(z), \qquad w_{g1}(s_{g1}, n_{g1}, z) = W_1(z) + n_{g1}V'(z) \tag{2}$$

Similarly, a global coordinate system $O_{g2}XY_{g2}Z$ and a local coordinate $C_{g2}s_{g2}n_{g2}z$ are assigned for the GFRP laminate 2 cross-section (Figure 5a). The through-thickness displacement fields at a Point with coordinates (n_{g2}, z) are depicted as v_{g2}, w_{g2} (Figure 5b).

Figure 5 Definitions of (a) Local coordinate system and (b) through-thickness displacement fields in the GFRP laminate 2 section

Displacement fields v_{g2}, w_{g2} can be assumed in terms of the governing displacement fields as

$$v_{g2}\left(s_{g2}, n_{g2}, z\right) = -V\left(z\right), \qquad w_{g2}\left(s_{g2}, n_{g2}, z\right) = W_2\left(z\right) + n_{g2}V'\left(z\right) \tag{3}$$

Through-thickness displacements in the adhesive layers 1 and 2:

A local coordinate $C_{a1}s_{a1}n_{a1}z$ is assigned for the adhesive layer 1 cross-section (Figure 6a). The through-thickness displacement fields at a Point with coordinates $\left(n_{a1}, z\right)$ are depicted as v_{a1}, w_{a1} (Figure 6b).

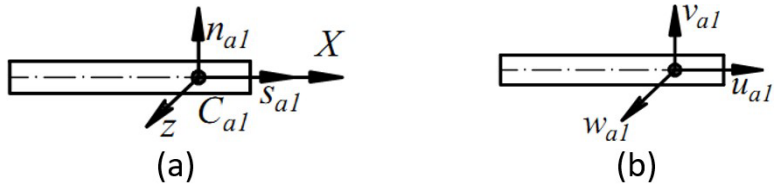

Figure 6 Definitions of (a) Local coordinate system and (b) through-thickness displacement fields in the Adhesive layer 1 section

Displacement fields v_{a1}, w_{a1} are linearly interpolated from the displacements at the uppermost steel fiber and those at the bottom of the GFRP laminate 1, i.e.,

$$\begin{aligned} v_{a1}\left(s_{a1}, n_{a1}, z\right) &= \left(\frac{1}{2} - \frac{n_{a1}}{t_{a1}}\right) v_s\left(s_s, \frac{t_f}{2}, z\right) + \left(\frac{1}{2} + \frac{n_{a1}}{t_{a1}}\right) v_{g1}\left(s_{g1}, -\frac{t_{g1}}{2}, z\right), \\ w_{a1}\left(s_{a1}, n_{a1}, z\right) &= \left(\frac{1}{2} - \frac{n_{a1}}{t_{a1}}\right) w_s\left(s_s, \frac{t_f}{2}, z\right) + \left(\frac{1}{2} + \frac{n_{a1}}{t_{a1}}\right) w_{g1}\left(s_{g1}, -\frac{t_{g1}}{2}, z\right) \end{aligned} \tag{4}$$

From Eqs. (1), by setting $n_s = t_f/2$, and from Eqs. (2), by setting $n_{g1} = -t_{g1}/2$, then substituting the results into Eqs. (4), one has

$$\begin{aligned} &v_{a1}\left(s_{a1}, n_{a1}, z\right) = -V\left(z\right), \\ &w_{a1}\left(s_{a1}, n_{a1}, z\right) = \left(\frac{1}{2} - \frac{n_{a1}}{t_{a1}}\right) W\left(z\right) + \left(\frac{1}{2} + \frac{n_{a1}}{t_{a1}}\right) W_1\left(z\right) + \left[\frac{t_f - t_{g1}}{4} - \frac{\left(t_f + t_{g1}\right) n_{a1}}{2t_{a1}}\right] V'\left(z\right) + \frac{h_b}{2}\left(\frac{1}{2} - \frac{n_{a1}}{t_{a1}}\right) \theta_x\left(z\right) \end{aligned} \tag{5}$$

Similarly, a local coordinate $C_{a2}s_{a2}n_{a2}z$ is assigned for the adhesive layer 2 cross-section (Figure 7a). The through-thickness displacement fields at a Point with coordinates $\left(n_{a2}, z\right)$ are depicted as v_{a2}, w_{a2} (Figure 7b).

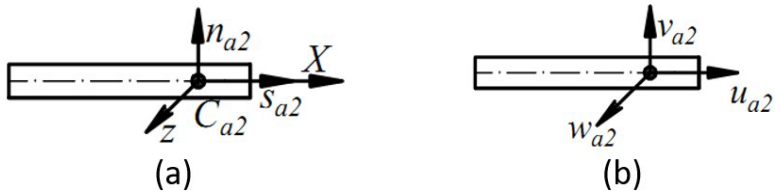

Figure 7 Definitions of (a) Local coordinate system and (b) through-thickness displacement fields in the Adhesive layer 2 section

Displacement fields v_{a2}, w_{a2} are linearly interpolated from the displacements lowermost steel fiber and those at the top of the GFRP laminate 2, i.e.,

$$\begin{aligned} v_{a2}\left(s_{a2}, n_{a2}, z\right) &= \left(\frac{1}{2}+\frac{n_{a2}}{t_{a2}}\right) v_s\left(s_s, -\frac{t_f}{2}, z\right) + \left(\frac{1}{2}-\frac{n_{a2}}{t_{a2}}\right) v_{g2}\left(s_{g2}, \frac{t_{g2}}{2}, z\right), \\ w_{a2}\left(s_{a2}, n_{a2}, z\right) &= \left(\frac{1}{2}+\frac{n_{a2}}{t_{a2}}\right) w_s\left(s_s, -\frac{t_f}{2}, z\right) + \left(\frac{1}{2}-\frac{n_{a2}}{t_{a2}}\right) w_{g2}\left(s_{g2}, \frac{t_{g2}}{2}, z\right) \end{aligned} \tag{6}$$

From Eqs. (1), by setting $n_s = -t_f/2$, and from Eqs. (2), by setting $n_{g2} = t_{g2}/2$, then substituting the results into Eqs. (6), one has

$$\begin{aligned} v_{a2}\left(s_{a2}, n_{a2}, z\right) &= -V\left(z\right), \\ w_{a2}\left(s_{a2}, n_{a2}, z\right) &= \left(\frac{1}{2}+\frac{n_{a2}}{t_{a2}}\right) W\left(z\right) + \left(\frac{1}{2}-\frac{n_{a2}}{t_{a2}}\right) W_2\left(z\right) - \left[\frac{\left(t_f - t_{g2}\right)}{4} + \frac{\left(t_f + t_{g2}\right) n_{a2}}{2t_{a2}}\right] V'\left(z\right) - \frac{h_b}{2}\left(\frac{1}{2}+\frac{n_{a2}}{t_{a2}}\right)\theta_x\left(z\right) \end{aligned} \tag{7}$$

3.3 Develop strain fields

The longitudinal normal strains and in-plane shear strains in the steel beam, GFRP laminate 1 and GFRP laminate 2 are assumed as

$$\varepsilon_i = \frac{\partial w_i}{\partial z}, \qquad \gamma_{i,sz} = \frac{\partial u_i}{\partial z} + \frac{\partial w_i}{\partial s_i} \tag{8}$$

in which subscript $i = s$ for steel, $i = g1$ for GFRP laminate 1 and $i = g2$ for GFRP laminate 2. From Eqs. (1), by substituting into Eqs. (8), the strain fields in the steel beam can be obtained as

$$\varepsilon_s = W'\left(z\right) + n_s \cos\alpha\left(s_s\right) V''\left(z\right) - y\left(s_s\right)\theta_x'\left(z\right), \qquad \gamma_{s,sz} = \sin\alpha\left(s_1\right)\left\{V'\left(z\right) - \theta_x\left(z\right)\right\} \tag{9}$$

Similarly, from Eqs. (2), by substituting into Eqs. (8), the strain fields in the GFRP laminate 1 are obtained as

$$\varepsilon_{g1} = \varepsilon_{g1,zz}^{*} + n_{g1}\kappa_{g1,zz}^{*}, \qquad \gamma_{g1,sz} = 0 \tag{10}$$

in which

$$\varepsilon_{g1,zz}^{*} = W_1'\left(z\right), \qquad \kappa_{g1,zz}^{*} = V''\left(z\right) \tag{11}$$

Also, from Eqs. (3), by substituting into Eqs. (8), the strain fields in the GFRP laminate 2 are obtained as

$$\varepsilon_{g2} = \varepsilon_{g2,zz}^{*} + n_{g2}\kappa_{g2,zz}^{*}, \qquad \gamma_{g2,sz} = 0 \tag{12}$$

in which

$$\varepsilon_{g2,zz}^{*} = W_2'\left(z\right), \qquad \kappa_{g2,zz}^{*} = V''\left(z\right) \tag{13}$$

The shear strain field in the adhesive layers can be assumed as

$$\gamma_{i,nz} = \frac{\partial v_i}{\partial z} + \frac{\partial w_i}{\partial n_i} \tag{14}$$

where subscript $i = a1$ is denoted for the adhesive layer 1 while $i = a2$ is for the adhesive layer 2. From Eqs. (5), by substituting into Eqs. (14), the shear strain field in Adhesive layer 1 can be simplified as

$$\gamma_{a1,nz} = -\frac{1}{t_{a1}} W\left(z\right) + \frac{1}{t_{a1}} W_1\left(z\right) - \frac{\left(2t_{a1} + t_f + t_{g1}\right)}{2t_{a1}} V'\left(z\right) - \frac{h_b}{2t_{a1}}\theta_x\left(z\right) \tag{15}$$

Similarly, from Eqs. (7), by substituting into Eqs. (14), the shear strain in Adhesive layer 2 is obtained as

$$\gamma_{a2,nz}=\frac{1}{t_{a2}}W\left(z\right)-\frac{1}{t_{a2}}W_2\left(z\right)-\frac{\left(2t_{a2}+t_f+t_{g2}\right)}{2t_{a2}}V'\left(z\right)-\frac{h_b}{2t_{a2}}\theta_x\left(z\right) \tag{16}$$

3.4 Develop stress and shell stress resultant fields

The steel beam is assumed as a linearly elastic isotropic material with a modulus of elasticity E_s and a Poisson's ratio of μ. The adhesive layers are also assumed as linearly elastic materials with a shear modulus G_{ai}, where i can be 1 or 2 that denotes for Adhesive layer 1 or adhesive layer 2, respectively (Figure 1a). The stress fields corresponding to the strain fields developed in Eqs. (9), (15), and (16) maybe expressed as

$$\sigma_s=E_s\varepsilon_s,\qquad \tau_{s,sz}=G_s\gamma_{s,sz},\qquad \gamma_{a1,nz}=G_{a1}\gamma_{a1,nz},\quad \gamma_{a2,nz}=G_{a2}\gamma_{a2,nz} \tag{17}$$

GFRP laminates 1 and 2 are assumed as linearly elastic orthotropic materials and they are symmetrically balanced laminates stacked by n orthotropic laminae, of which the k^{th} lamina ($k=1,2,...,n$) has a longitudinal modulus of elasticity $E_{k,z}$, a lateral modulus of elasticity $E_{k,s}$, a shear modulus $G_{k,sz}$, and Poisson's ratio $v_{k,zs}$, $v_{k,sz}$ (Appendix 1). Constitutive equations of the GFRP laminates 1 and 2 may be expressed as

$$\begin{cases} N^*_{gi,zz}=\overline{A}_{gi,11}\varepsilon^*_{gi,zz} \\ M^*_{gi,zz}=\overline{D}_{gi,11}\kappa^*_{gi,zz} \end{cases},\qquad \left(i=1,2\right) \tag{18}$$

in which $N^*_{gi,zz}$, $M^*_{gi,zz}$, ($i=1,2$) are shell stress resultants in GFRP laminate i and they are respectively obtained by integrating stresses $\sigma_{gi,zz}$, $n_{gi}\sigma_{gi,zz}$ from $n_{gi}=-t_{gi}/2$ to $n_{gi}=t_{gi}/2$, where $\sigma_{gi,zz}$ is the longitudinal normal stress field in the GFRP laminate i, ($i=1,2$) and n_{gi} is the normal-to-tangent axis of the contour measured from the contour of the GFRP laminate i, ($i=1,2$). Plate stiffnesses $\overline{A}_{gi,11},\overline{D}_{gi,11}$ in Eqs. (18) have been evaluated and presented in Appendix 1.

3.5 Develop total potential energy

The total potential energy π of the system is contributed by the internal strain energy π_U and the load potential loss π_V, i.e.,

$$\pi=\pi_U+\pi_V=0 \tag{19}$$

where the internal strain energy U is contributed by

$$\begin{aligned}\pi_U=\frac{1}{2}\Bigg[&\int_0^L\int_{A_s}\varepsilon_s\sigma_s dA_s dz+\int_0^L\int_{A_s}\gamma_{s,sz}\tau_{s,sz}dA_s dz+\int_0^L\int_0^b\varepsilon^*_{g1,zz}N^*_{g1,zz}dxdz+\int_0^L\int_0^b\kappa^*_{g1,zz}M^*_{g1,zz}dxdz\\&+\int_0^L\int_{A_{a1}}\left(\gamma_{a1,zn}\tau_{a1,zn}\right)dA_{a2}dz+\int_0^L\int_0^b\varepsilon^*_{g2,zz}N^*_{g2,zz}dxdz+\int_0^L\int_0^b\kappa^*_{g2,zz}M^*_{g2,zz}dxdz+\int_0^L\int_{A_{a2}}\left(\gamma_{a2,zn}\tau_{a2,zn}\right)dA_{a2}dz\Bigg]\end{aligned} \tag{20}$$

From Eqs. (17) and (18), by substituting into Eq. (20), one obtains

$$\begin{aligned}\pi_U=\frac{1}{2}\Bigg[&\int_0^L\int_{A_s}E_s\varepsilon_s^2dA_s dz+\int_0^L\int_{A_s}G_s\gamma_{s,sz}^2dA_s dz+\int_0^L\int_0^b\overline{A}_{g1,11}\varepsilon^2_{g1,zz}dxdz+\int_0^L\int_0^b\overline{D}_{g1,11}\kappa^2_{g1,zz}dxdz\\&+\int_0^L\int_{A_{a1}}G_{a1}\gamma^2_{a1,zn}dA_{a1}dz+\int_0^L\int_0^{b_2}\overline{A}_{g2,11}\varepsilon^2_{g2,zz}dxdz+\int_0^L\int_0^{b_2}\overline{D}_{g2,11}\kappa^2_{g2,zz}dxdz+\int_0^L\int_{A_{a2}}G_{a2}\gamma^2_{a2,zn}dA_{a2}dz\Bigg]\end{aligned} \tag{21}$$

From Eqs. (9), (10)-(13), (15), (16), by substituting into Eq. (21), by performing area integrals, and by arranging terms according to governing displacement fields, one obtains

$$\begin{aligned}\pi_U=\frac{1}{2}\int_0^L\Bigg[&E_sA_s\left(W'\right)^2+\left(\frac{G_{a1}A_{a1}}{t_{a1}^{\,2}}+\frac{G_{a2}A_{a2}}{t_{a2}^{\,2}}\right)W^2+\left(E_s\frac{2bt_f^3}{12}+\bar{D}_{g1,11}b_1+\bar{D}_{g2,11}b_2\right)\left(V''\right)^2\\&+\left(G_sh_wt_w+G_{a1}A_{a1}\frac{\left(2t_{a1}+t_f+t_{g1}\right)^2}{\left(2t_{a1}\right)^2}+G_{a2}A_{a2}\frac{\left(2t_{a2}+t_f+t_{g2}\right)^2}{\left(2t_{a2}\right)^2}\right)\left(V'\right)^2+E_s\left(\frac{bt_fh_b^2}{2}+\frac{t_wh_b^3}{12}\right)\theta_x'^2\\&+\left(G_sh_wt_w+\frac{G_{a1}A_{a1}h_b^2}{4t_{a1}^{\,2}}+\frac{G_{a2}A_{a2}h_b^2}{4t_{a2}^{\,2}}\right)\theta_x^{\,2}+\bar{A}_{g1,11}b_1\left(W_1'\right)^2+G_{a1}A_{a1}\left(\frac{1}{t_{a1}}\right)^2W_1^2+\bar{A}_{g2,11}b\left(W_2'\right)^2+G_{a2}A_{a2}\left(\frac{1}{t_{a2}}\right)^2W_2^{\,2}\\&-2G_sh_wt_wV'\theta_x+\left(G_{a1}A_{a1}\frac{\left(2t_{a1}+t_f+t_{g1}\right)}{t_{a1}^{\,2}}-G_{a2}A_{a2}\frac{\left(2t_{a2}+t_f+t_{g2}\right)}{t_{a2}^{\,2}}\right)WV'+\left(\frac{G_{a1}A_{a1}h_b}{t_{a1}^{\,2}}-\frac{G_{a2}A_{a2}h_b}{t_{a2}^{\,2}}\right)W\theta_x\\&+\left(G_{a1}A_{a1}\frac{\left(2t_{a1}+t_f+t_{g1}\right)h_b}{2t_{a1}^{\,2}}+G_{a2}A_{a2}\frac{\left(2t_{a2}+t_f+t_{g2}\right)h_b}{2t_{a2}^{\,2}}\right)V'\theta_x-2G_{a1}A_{a1}\left(\frac{1}{t_{a1}}\right)^2WW_1-2\frac{G_{a1}A_{a1}}{t_{a1}}\frac{\left(2t_{a1}+t_f+t_{g1}\right)}{2t_{a1}}W_1V'\\&-2G_{a1}A_{a1}\frac{1}{t_{a1}}\frac{h_b}{2t_{a1}}W_1\theta_x-2G_{a2}A_{a2}\left(\frac{1}{t_{a2}}\right)^2WW_2+2G_{a2}A_{a2}\frac{1}{t_{a2}}\frac{\left(2t_{a2}+t_f+t_{g2}\right)}{2t_{a2}}W_2V'+2G_{a2}A_{a2}\frac{1}{t_{a2}}\frac{h_b}{2t_{a2}}W_2\theta_x\Bigg]dz\end{aligned}\tag{22}$$

The load potential energy of the element may be contributed by end forces and distributed loads as follows

$$\pi_V=\pi_{V1}+\pi_{V2}\tag{23}$$

where π_{V1} is the load potential energy caused by end (internal) forces associated with the governing displacements at two member ends and it can be obtained as

$$\begin{aligned}\pi_{V1}=-\big[&N_z(0)W(0)+N_{z1}(0)W_1(0)+N_{z2}(0)W_2(0)+Q_y(0)V(0)+M_{xv}(0)V'(0)+M_{x\theta}(0)\theta_x(0)\\&-N_z(L)W(L)-N_{z1}(L)W_1(L)-N_{z2}(L)W_2(L)-Q_y(L)V(L)-M_{xv}(L)V'(L)-M_{x\theta}(L)\theta_x(L)\big]\end{aligned}\tag{24}$$

while the load potential energy caused by a distributed load $q_y(z)$:

$$\pi_{V2}=-\int_0^L q_y(z)V(z)dz\tag{25}$$

3.6 Develop a finite element formulation

Nodal displacement vector:

The nodal displacement vector of the present element formulation, denoted as $\{\Delta\}_{12\times1}$, is assumed as

$$\{\Delta\}_{1\times12}^T=\left\langle W^{(0)}\quad W_1^{(0)}\quad W_2^{(0)}\quad V^{(0)}\quad V'^{(0)}\quad\theta_x^{(0)}\;\middle|\;W^{(L)}\quad W_1^{(L)}\quad W_2^{(L)}\quad V^{(L)}\quad V'^{(L)}\quad\theta_x^{(L)}\right\rangle\tag{26}$$

in which, symbols (0) and (L) denote for the coordinates at $Z=0$ and $Z=L$, respectively, of the present finite element. The nodal displacements in Eq. (26) are defined in Figure 8.

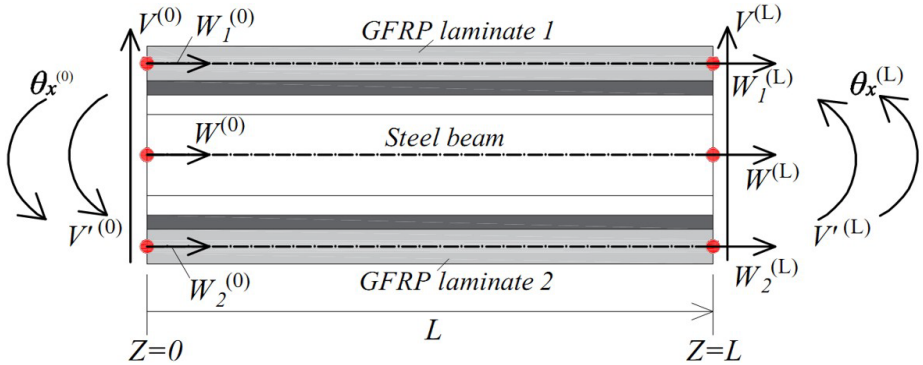

Figure 8 Nodal displacement vector of the present finite element

Interpolated governing displacement fields:

The governing displacement fields at a coordinate Z in the element ($0 \le Z \le L$) are assumed to be interpolated from the nodal displacement vector as follows.

$$\begin{aligned} &W(z) = \left\langle \mathbf{Z}_w \right\rangle_{1\times 12}^T \left\{ \mathbf{\Delta} \right\}_{12\times 1}, \; W_1(z) = \left\langle \mathbf{Z}_{w1} \right\rangle_{1\times 12}^T \left\{ \mathbf{\Delta} \right\}_{12\times 1}, \qquad W_2(z) = \left\langle \mathbf{Z}_{w2} \right\rangle_{1\times 12}^T \left\{ \mathbf{\Delta} \right\}_{12\times 1}, \\ &V(z) = \left\langle \mathbf{Z}_v \right\rangle_{1\times 12}^T \left\{ \mathbf{\Delta} \right\}_{12\times 1}, \quad \theta_x(z) = \left\langle \mathbf{Z}_{\theta x} \right\rangle_{1\times 12}^T \left\{ \mathbf{\Delta} \right\}_{12\times 1} \end{aligned} \tag{27}$$

where vectors $\left\langle \mathbf{Z}_w \right\rangle_{1\times 12}^T, \left\langle \mathbf{Z}_{w1} \right\rangle_{1\times 12}^T, \left\langle \mathbf{Z}_{w2} \right\rangle_{1\times 12}^T, \left\langle \mathbf{Z}_v \right\rangle_{1\times 12}^T, \left\langle \mathbf{Z}_{\theta x} \right\rangle_{1\times 12}^T$ are shape functions, taken as

$$\begin{aligned} &\left\langle \mathbf{Z}_w \right\rangle_{1\times 12}^T = \left\langle \mathbf{F}_l(z) \right\rangle_{1\times 2}^T \left[\mathbf{\rho}_w \right]_{2\times 12}, \qquad \left\langle \mathbf{Z}_{w1} \right\rangle_{1\times 12}^T = \left\langle \mathbf{F}_l(z) \right\rangle_{1\times 2}^T \left[\mathbf{\rho}_{w1} \right]_{2\times 12}, \quad \left\langle \mathbf{Z}_{w2} \right\rangle_{1\times 12}^T = \left\langle \mathbf{F}_l(z) \right\rangle_{1\times 2}^T \left[\mathbf{\rho}_{w2} \right]_{2\times 12} \\ &\left\langle \mathbf{Z}_v \right\rangle_{1\times 12}^T = \left\langle \mathbf{F}_c(z) \right\rangle_{1\times 4}^T \left[\mathbf{\rho}_v \right]_{4\times 12}, \qquad \left\langle \mathbf{Z}_{\theta x} \right\rangle_{1\times 12}^T = \left\langle \mathbf{F}_l(z) \right\rangle_{1\times 2}^T \left[\mathbf{\rho}_{\theta x} \right]_{2\times 12} \end{aligned} \tag{28}$$

In Eqs. (28), the following linear and cubic interpolation functions have been introduced

$$\begin{aligned} &\left\langle \mathbf{F}_l(z) \right\rangle_{1\times 2}^T = \left\langle 1 - z/L \;\vdots\; z/L \right\rangle \\ &\left\langle \mathbf{F}_c(z) \right\rangle_{1\times 4}^T = \left\langle 1 - 3(z/L)^2 + 2(z/L)^3 \;\vdots\; z - 2\left(z^2/L\right) + \left(z^3/L^2\right) \;\vdots\; 3(z/L)^2 - 2(z/L)^3 \;\vdots\; z^3/L^2 - z^2/L \right\rangle \end{aligned} \tag{29}$$

and the following index matrices have been defined

$$\begin{aligned} \left[\mathbf{\rho}_w \right]_{2\times 12} &= \left[\begin{array}{cccccc:cccccc} 1 & 0 & 0 & 0 & 0 & 0 & 0 & 0 & 0 & 0 & 0 & 0 \\ 0 & 0 & 0 & 0 & 0 & 0 & 1 & 0 & 0 & 0 & 0 & 0 \end{array} \right] \\ \left[\mathbf{\rho}_{w1} \right]_{2\times 12} &= \left[\begin{array}{cccccc:cccccc} 0 & 1 & 0 & 0 & 0 & 0 & 0 & 0 & 0 & 0 & 0 & 0 \\ 0 & 0 & 0 & 0 & 0 & 0 & 0 & 1 & 0 & 0 & 0 & 0 \end{array} \right] \\ \left[\mathbf{\rho}_{w2} \right]_{2\times 12} &= \left[\begin{array}{cccccc:cccccc} 0 & 0 & 1 & 0 & 0 & 0 & 0 & 0 & 0 & 0 & 0 & 0 \\ 0 & 0 & 0 & 0 & 0 & 0 & 0 & 0 & 1 & 0 & 0 & 0 \end{array} \right] \\ \left[\mathbf{\rho}_v \right]_{4\times 12} &= \left[\begin{array}{cccccc:cccccc} 0 & 0 & 0 & 1 & 0 & 0 & 0 & 0 & 0 & 0 & 0 & 0 \\ 0 & 0 & 0 & 0 & 1 & 0 & 0 & 0 & 0 & 0 & 0 & 0 \\ 0 & 0 & 0 & 0 & 0 & 0 & 0 & 0 & 0 & 1 & 0 & 0 \\ 0 & 0 & 0 & 0 & 0 & 0 & 0 & 0 & 0 & 0 & 1 & 0 \end{array} \right] \\ \left[\mathbf{\rho}_{\theta x} \right]_{2\times 12} &= \left[\begin{array}{cccccc:cccccc} 0 & 0 & 0 & 0 & 0 & 1 & 0 & 0 & 0 & 0 & 0 & 0 \\ 0 & 0 & 0 & 0 & 0 & 0 & 0 & 0 & 0 & 0 & 0 & 1 \end{array} \right] \end{aligned} \tag{30}$$

Expression of total potential energy of the system:

From Eqs. (27), by substituting into Eqs. (22) and re-arranging terms, one obtains

$$\pi = \pi_U + \pi_{V1} + \pi_{V2} = \frac{1}{2} \left\langle \mathbf{\Delta} \right\rangle_{1\times 12}^T \left[\mathbf{K} \right]_{12\times 12} \left\{ \mathbf{\Delta} \right\}_{12\times 1} - \left\langle \mathbf{\Delta} \right\rangle_{1\times 12}^T \left\{ \mathbf{P}_1 \right\}_{12\times 1} - \left\langle \mathbf{\Delta} \right\rangle_{1\times 12}^T \left\{ \mathbf{P}_2 \right\}_{12\times 1} \tag{31}$$

In which $\left[\mathbf{K} \right]_{12\times 12}$ is the element stiffness matrix and it can be obtained as

$$\left[\mathbf{K} \right]_{12\times 12} = \left[\mathbf{k}_1 + \mathbf{k}_2 + \mathbf{k}_3 + \mathbf{k}_4 + \mathbf{k}_5 + \mathbf{k}_6 + \mathbf{k}_7 + \mathbf{k}_8 + \mathbf{k}_9 + \mathbf{k}_{10} + \mathbf{k}_{11} + \mathbf{k}_{12} + \mathbf{k}_{13} + \mathbf{k}_{14} + \mathbf{k}_{15} + \mathbf{k}_{16} + \mathbf{k}_{17} + \mathbf{k}_{18} + \mathbf{k}_{19} \right]_{12\times 12} \tag{32}$$

Where the component stiffness matrices $\left[\mathbf{k}_i \right]_{12\times 12}$, $i = 1,2,...,19$, depends on sectional and material properties and they are determined as

$$
\begin{aligned}
&[\mathbf{k}_1]=E_s A_s[\boldsymbol{\rho}_w]_{12\times2}^T[\mathbf{H}_{ll,1}]_{2\times2}[\boldsymbol{\rho}_w]_{2\times12}, \qquad [\mathbf{k}_2]=E_s\left(\frac{bt_f h_b^2}{2}+\frac{t_w h_w^3}{12}\right)[\boldsymbol{\rho}_{\theta x}]_{12\times2}^T[\mathbf{H}_{ll,1}]_{2\times2}[\boldsymbol{\rho}_{\theta x}]_{2\times12},\\
&[\mathbf{k}_3]=\left(E_s\frac{2bt_f^3}{12}+\bar{D}_{g1,11}b+\bar{D}_{g2,11}b\right)[\boldsymbol{\rho}_v]_{12\times4}^T[\mathbf{H}_{cc,2}]_{4\times4}[\boldsymbol{\rho}_v]_{4\times12},\\
&[\mathbf{k}_4]=\left(G_s h_w t_w+G_{a1}A_{a1}\frac{\left(2t_{a1}+t_f+t_{g1}\right)^2}{\left(2t_{a1}\right)^2}+G_{a2}A_{a2}\frac{\left(2t_{a2}+t_f+t_{g2}\right)^2}{\left(2t_{a2}\right)^2}\right)[\boldsymbol{\rho}_v]_{12\times4}^T[\mathbf{H}_{cc,1}]_{4\times4}[\boldsymbol{\rho}_v]_{4\times12},\\
&[\mathbf{k}_5]=\left(G_s h_w t_w+\frac{G_{a1}A_{a1}h_b^2}{4t_{a1}^2}+\frac{G_{a2}A_{a2}h_b^2}{4t_{a2}^2}\right)[\boldsymbol{\rho}_{\theta x}]_{12\times2}^T[\mathbf{H}_{ll}]_{2\times2}[\boldsymbol{\rho}_{\theta x}]_{2\times12},\\
&[\mathbf{k}_6]=\left[-G_s h_w t_w+G_{a1}A_{a1}\frac{\left(2t_{a1}+t_f+t_{g1}\right)h_b}{4t_{a1}^2}+G_{a2}A_{a2}\frac{\left(2t_{a2}+t_f+t_{g2}\right)h_b}{4t_{a2}^2}\right]\left([\boldsymbol{\rho}_v]_{12\times4}^T[\mathbf{H}_{cl,1o}]_{4\times2}[\boldsymbol{\rho}_{\theta x}]_{2\times12}+[\boldsymbol{\rho}_{\theta x}]_{12\times2}^T[\mathbf{H}_{lc,o1}]_{2\times4}[\boldsymbol{\rho}_v]_{4\times12}\right),\\
&[\mathbf{k}_7]=+\bar{A}_{g1,11}b[\boldsymbol{\rho}_{w1}]_{12\times2}^T[\mathbf{H}_{ll,1}]_{2\times2}[\boldsymbol{\rho}_{w1}]_{2\times12}, \qquad [\mathbf{k}_8]=\left(\frac{G_{a1}A_{a1}}{t_{a1}^2}+\frac{G_{a2}A_{a2}}{t_{a2}^2}\right)[\boldsymbol{\rho}_w]_{12\times2}^T[\mathbf{H}_{ll}]_{2\times2}[\boldsymbol{\rho}_w]_{2\times12},\\
&[\mathbf{k}_9]=+\frac{1}{2}\left(G_{a1}A_{a1}\frac{\left(2t_{a1}+t_f+t_{g1}\right)}{t_{a1}^2}-G_{a2}A_{a2}\frac{\left(2t_{a2}+t_f+t_{g2}\right)}{t_{a2}^2}\right)\left([\boldsymbol{\rho}_v]_{12\times4}^T[\mathbf{H}_{cl,1o}]_{4\times2}[\boldsymbol{\rho}_w]_{2\times12}+[\boldsymbol{\rho}_w]_{12\times2}^T[\mathbf{H}_{lc,o1}]_{2\times4}[\boldsymbol{\rho}_v]_{4\times12}\right),\\
&[\mathbf{k}_{10}]=\frac{1}{2}\left(\frac{G_{a1}A_{a1}h_b}{t_{a1}^2}-\frac{G_{a2}A_{a2}h_b}{t_{a2}^2}\right)\left([\boldsymbol{\rho}_w]_{12\times2}^T[\mathbf{H}_{ll}]_{2\times2}[\boldsymbol{\rho}_{\theta x}]_{2\times12}+[\boldsymbol{\rho}_{\theta x}]_{12\times2}^T[\mathbf{H}_{ll}]_{2\times2}[\boldsymbol{\rho}_w]_{2\times12}\right),\\
&[\mathbf{k}_{11}]=+G_{a1}A_{a1}\left(\frac{1}{t_{a1}}\right)^2[\boldsymbol{\rho}_{w1}]_{12\times2}^T[\mathbf{H}_{ll}]_{2\times2}[\boldsymbol{\rho}_{w1}]_{2\times12}, \quad [\mathbf{k}_{12}]=-G_{a1}A_{a1}\left(\frac{1}{t_{a1}}\right)^2\left([\boldsymbol{\rho}_w]_{12\times2}^T[\mathbf{H}_{ll}]_{2\times2}[\boldsymbol{\rho}_{w1}]_{2\times12}+[\boldsymbol{\rho}_{w1}]_{12\times2}^T[\mathbf{H}_{ll}]_{2\times2}[\boldsymbol{\rho}_w]_{2\times12}\right),\\
&[\mathbf{k}_{13}]=-G_{a1}A_{a1}\frac{1}{t_{a1}}\frac{\left(2t_{a1}+t_f+t_{g1}\right)}{2t_{a1}}\left([\boldsymbol{\rho}_{w1}]_{12\times2}^T[\mathbf{H}_{lc,o1}]_{2\times4}[\boldsymbol{\rho}_v]_{4\times12}+[\boldsymbol{\rho}_v]_{12\times4}^T[\mathbf{H}_{cl,1o}]_{4\times2}[\boldsymbol{\rho}_{w1}]_{2\times12}\right),\\
&[\mathbf{k}_{14}]=-\frac{G_{a1}A_{a1}}{t_{a1}}\frac{h_b}{2t_{a1}}\left([\boldsymbol{\rho}_{w1}]_{12\times2}^T[\mathbf{H}_{ll}]_{2\times2}[\boldsymbol{\rho}_{\theta x}]_{2\times12}+[\boldsymbol{\rho}_{\theta x}]_{12\times2}^T[\mathbf{H}_{ll}]_{2\times2}[\boldsymbol{\rho}_{w1}]_{2\times12}\right),\\
&[\mathbf{k}_{15}]=+\bar{A}_{g2,11}b[\boldsymbol{\rho}_{w2}]_{12\times2}^T[\mathbf{H}_{ll,1}]_{2\times2}[\boldsymbol{\rho}_{w2}]_{2\times12}, \qquad [\mathbf{k}_{16}]=+G_{a2}A_{a2}\left(\frac{1}{t_{a2}}\right)^2[\boldsymbol{\rho}_{w2}]_{12\times2}^T[\mathbf{H}_{ll}]_{2\times2}[\boldsymbol{\rho}_{w2}]_{2\times12},\\
&[\mathbf{k}_{17}]=-G_{a2}A_{a2}\left(\frac{1}{t_{a2}}\right)^2\left([\boldsymbol{\rho}_w]_{12\times2}^T[\mathbf{H}_{ll}]_{2\times2}[\boldsymbol{\rho}_{w2}]_{2\times12}+[\boldsymbol{\rho}_{w2}]_{12\times2}^T[\mathbf{H}_{ll}]_{2\times2}[\boldsymbol{\rho}_w]_{2\times12}\right),\\
&[\mathbf{k}_{18}]=+\frac{G_{a2}A_{a2}}{t_{a2}}\frac{\left(2t_{a2}+t_f+t_{g2}\right)}{2t_{a2}}\left([\boldsymbol{\rho}_{w2}]_{12\times2}^T[\mathbf{H}_{lc,o1}]_{2\times4}[\boldsymbol{\rho}_v]_{4\times12}+[\boldsymbol{\rho}_v]_{12\times4}^T[\mathbf{H}_{cl,1o}]_{4\times2}[\boldsymbol{\rho}_{w2}]_{2\times12}\right),\\
&[\mathbf{k}_{19}]=+\frac{G_{a2}A_{a2}}{t_{a2}}\frac{h_b}{2t_{a2}}\left([\boldsymbol{\rho}_{w2}]_{12\times2}^T[\mathbf{H}_{ll}]_{2\times2}[\boldsymbol{\rho}_{\theta x}]_{2\times12}+[\boldsymbol{\rho}_{\theta x}]_{12\times2}^T[\mathbf{H}_{ll}]_{2\times2}[\boldsymbol{\rho}_{w2}]_{2\times12}\right)
\end{aligned}
\tag{33}
$$

where $A_s=2bt_f+(h-2t_f)t_w$, $A_{a1}=t_{a1}b_1$, $A_{a2}=t_{a2}b_2$. The terms in Eq. (33) including the element length L has been grouped in the following matrices.

$$
\begin{aligned}
&[\mathrm{H}_{ll}]_{2\times2}=\frac{L}{6}\begin{bmatrix}2&1\\1&2\end{bmatrix}, \qquad [\mathrm{H}_{ll,1}]_{2\times2}=\frac{1}{L}\begin{bmatrix}1&-1\\-1&1\end{bmatrix},\\
&[\mathrm{H}_{lc,o1}]_{2\times4}=\frac{1}{12}\begin{bmatrix}-6&L&6&-L\\-6&-L&6&L\end{bmatrix}, \qquad [\mathrm{H}_{cl,1o}]_{4\times2}=[\mathrm{H}_{lc,o1}]_{4\times2}^T\\
&[\mathrm{H}_{cc,1}]_{4\times4}=\frac{1}{30L}\begin{bmatrix}36&3L&-36&3L\\3L&4L^2&-3L&-L^2\\-36&-3L&36&-3L\\3L&-L^2&-3L&4L^2\end{bmatrix}, \qquad [\mathrm{H}_{cc,2}]_{4\times4}=\frac{1}{L^3}\begin{bmatrix}12&6L&-12&6L\\6L&4L^2&-6L&2L^2\\-12&-6L&12&-6L\\6L&2L^2&-6L&4L^2\end{bmatrix},
\end{aligned}
\tag{34}
$$

Vector $\{\mathbf{P}_1\}_{12\times1}$ is the nodal force vector of the finite element and it is obtained from Eq. (24) as

$$
\langle \mathrm{P}_1\rangle_{1\times12}^T=\left\langle N_z^{(0)} \quad N_{z1}^{(0)} \quad N_{z2}^{(0)} \quad Q_y^{(0)} \quad M_{xV}^{(0)} \quad M_{x\theta}^{(0)} \;\vdots\; N_z^{(L)} \quad N_{z1}^{(L)} \quad N_{z2}^{(L)} \quad Q_y^{(L)} \quad M_{xV}^{(L)} \quad M_{x\theta}^{(L)}\right\rangle \tag{35}
$$

Also, $\{\mathbf{P}_2\}_{12\times1}$ is the equivalent nodal force vector of the element and it can be obtained by substituting $V(z)$ of Eq. (27) into Eq. (25) as

$$\{\mathrm{P}_2\}_{12\times1} = \int_L q_y(z)\{\mathrm{Z}_v\}_{12\times1}dz \tag{36}$$

Formulation of the present finite element:

From Eq. (31), by applying the first variational principle with respect to the nodal displacement vector $\{\boldsymbol{\Delta}\}_{12\times1}$ and noting the system stationary condition at equilibrium condition (i.e. $\delta\pi = 0$), a finite element formulation can be obtained as

$$[\mathbf{K}]_{12\times12}\{\boldsymbol{\Delta}\}_{12\times1} = \{\mathbf{P}_1\}_{12\times1} + \{\mathbf{P}_2\}_{12\times1} \tag{37}$$

where $[\mathbf{K}]_{12\times12}, \{\mathbf{P}_1\}_{12\times1}, \{\mathbf{P}_2\}_{12\times1}$ have been defined in Eqs. (32)-(36).

4 Development of THREE other finite element formulations

The finite element formulation (FE) developed in the previous section is for a general case in which the steel beam element is strengthened with 2 GFRP laminates bonded to the top and bottom flanges (Figure 1a,b). For three other cases in which the steel beam element is strengthened with a top GFRP laminate (Figure 1c), a bottom GFRP laminate (Figure 1d), or not strengthened (Figure 1e), simplifications of the general FE formulation can be made to derive finite element formulations for the cases, as presented in the following.

4.1 A steel beam element strengthened with a GFRP laminate bonded to the top flange

From the general FE formulation developed in Section 3, by eliminating all variables regarding to GFRP laminate 2 and adhesive layer 2, one obtains a steel beam element that is only strengthened with a top GFRP laminate. In such a case, the governing displacements of the system include $W(z), W_1(z), V(z), \theta_x(z)$ and thus the finite element formulation can be obtained as

$$[\mathbf{K}]_{10\times10}\{\boldsymbol{\Delta}\}_{10\times1} = \{\mathbf{P}_1\}_{10\times1} + \{\mathbf{P}_2\}_{10\times1} \tag{38}$$

in which $[\mathbf{K}]_{10\times10}, \{\boldsymbol{\Delta}\}_{10\times1}, \{\mathbf{P}_1\}_{10\times1}, \{\mathbf{P}_2\}_{10\times1}$ are the element stiffness matrix, nodal displacement vector, end force vector and equivalent load vector, respectively and they are expressed as

$$\begin{aligned}
&\{\boldsymbol{\Delta}\}_{1\times10}^T = \left\langle W^{(0)} \quad W_1^{(0)} \quad V^{(0)} \quad V'^{(0)} \quad \theta_x^{(0)} \;\vdots\; W^{(L)} \quad W_1^{(L)} \quad V^{(L)} \quad V'^{(L)} \quad \theta_x^{(L)} \right\rangle \\
&[\mathbf{K}]_{10\times10} = [\mathbf{k}_1 + \mathbf{k}_2 + \mathbf{k}_3 + \mathbf{k}_4 + \mathbf{k}_5 + \mathbf{k}_6 + \mathbf{k}_7 + \mathbf{k}_8 + \mathbf{k}_9 + \mathbf{k}_{10} + \mathbf{k}_{11} + \mathbf{k}_{12} + \mathbf{k}_{13} + \mathbf{k}_{14}]_{10\times10} \\
&\langle \mathbf{P}_1 \rangle_{1\times10}^T = \left\langle N_z^{(0)} \quad N_{z1}^{(0)} \quad Q_y^{(0)} \quad M_{xV}^{(0)} \quad M_{x\theta}^{(0)} \;\vdots\; N_z^{(L)} \quad N_{z1}^{(L)} \quad Q_y^{(L)} \quad M_{xV}^{(L)} \quad M_{x\theta}^{(L)} \right\rangle \\
&\{\mathbf{P}_2\}_{10\times1} = \int_L q_y(z)\{\mathbf{Z}_v\}_{10\times1}dz
\end{aligned} \tag{39}$$

where the component stiffnesses $[\mathbf{k}_i]_{12\times12}$, $i = 1,2,...,14$ and vector $\{\mathbf{Z}_v\}_{10\times1}$ can be found in Appendix A2.1.

4.2 A steel beam element strengthened with a GFRP laminate bonded to the bottom flange

Again, from the general FE formulation in Section 3, by eliminating all parameters regarding to GFRP laminate 1 and adhesive layer 1, one obtains a steel beam element that is only strengthened with a bottom GFRP laminate. In this case, the governing displacements of the system are $W(z), W_2(z), V(z), \theta_x(z)$ and thus the finite element formulation can be expressed as

$$[\mathbf{K}]_{10\times10}\{\boldsymbol{\Delta}\}_{10\times1} = \{\mathbf{P}_1\}_{10\times1} + \{\mathbf{P}_2\}_{10\times1} \tag{40}$$

in which $[\mathbf{K}]_{10\times10}, \{\boldsymbol{\Delta}\}_{10\times1}, \{\mathbf{P}_1\}_{10\times1}, \{\mathbf{P}_2\}_{10\times1}$ are the element stiffness matrix, nodal displacement vector, end force vector and equivalent load vector, respectively and they are determined as

$$\begin{aligned}
&\{\boldsymbol{\Delta}\}_{1\times10}^{T} = \left\langle W^{(0)} \quad W_2^{(0)} \quad V^{(0)} \quad V'^{(0)} \quad \theta_x^{(0)} \;\vdots\; W^{(L)} \quad W_2^{(L)} \quad V^{(L)} \quad V'^{(L)} \quad \theta_x^{(L)} \right\rangle \\
&[\mathbf{K}]_{10\times10} = [\mathbf{k}_1 + \mathbf{k}_2 + \mathbf{k}_3 + \mathbf{k}_4 + \mathbf{k}_5 + \mathbf{k}_6 + \mathbf{k}_7 + \mathbf{k}_8 + \mathbf{k}_9 + \mathbf{k}_{10} + \mathbf{k}_{11} + \mathbf{k}_{12} + \mathbf{k}_{13} + \mathbf{k}_{14}]_{10\times10} \\
&\langle \mathbf{P}_1 \rangle_{1\times10}^{T} = \left\langle N_z^{(0)} \quad N_{z2}^{(0)} \quad Q_y^{(0)} \quad M_{xV}^{(0)} \quad M_{x\theta}^{(0)} \;\vdots\; N_z^{(L)} \quad N_{z2}^{(L)} \quad Q_y^{(L)} \quad M_{xV}^{(L)} \quad M_{x\theta}^{(L)} \right\rangle \\
&\{\mathbf{P}_2\}_{10\times1} = \int_L q_y(z)\{\mathbf{Z}_v\}_{10\times1} dz
\end{aligned} \tag{41}$$

the component stiffnesses $[\mathbf{k}_i]_{12\times12}$, $i = 1,2,...,14$ and vector $\{\mathbf{Z}_v\}_{10\times1}$ can be found in Appendix A2.2.

4.3 A steel beam element is not strengthened (i.e., a bare steel element)

From the general FE formulation in Section 3, by eliminating all parameters regarding to GFRP laminates 1 and 2 and adhesive layers 1 and 2, one obtains a steel beam element that is not strengthened. The governing displacements of the system are $W(z), V(z), \theta_x(z)$ and the finite element formulation is obtained as

$$[\mathbf{K}]_{8\times8}\{\boldsymbol{\Delta}\}_{8\times1} = \{\mathbf{P}_1\}_{8\times1} + \{\mathbf{P}_2\}_{8\times1} \tag{42}$$

in which $[\mathbf{K}]_{8\times8}, \{\boldsymbol{\Delta}\}_{8\times1}, \{\mathbf{P}_1\}_{8\times1}, \{\mathbf{P}_2\}_{8\times1}$ are the element stiffness matrix, nodal displacement vector, end force vector and equivalent load vector, respectively and they are determined as

$$\begin{aligned}
&\{\boldsymbol{\Delta}\}_{1\times8}^{T} = \left\langle W^{(0)} \quad V^{(0)} \quad V'^{(0)} \quad \theta_x^{(0)} \;\vdots\; W^{(L)} \quad V^{(L)} \quad V'^{(L)} \quad \theta_x^{(L)} \right\rangle \\
&[\mathbf{K}]_{8\times8} = [\mathbf{k}_1 + \mathbf{k}_2 + \mathbf{k}_3 + \mathbf{k}_4 + \mathbf{k}_5 + \mathbf{k}_6 + \mathbf{k}_7 + \mathbf{k}_8 + \mathbf{k}_9 + \mathbf{k}_{10} + \mathbf{k}_{11} + \mathbf{k}_{12} + \mathbf{k}_{13} + \mathbf{k}_{14}]_{8\times8} \\
&\langle \mathbf{P}_1 \rangle_{1\times8}^{T} = \left\langle N_z^{(0)} \quad Q_y^{(0)} \quad M_{xV}^{(0)} \quad M_{x\theta}^{(0)} \;\vdots\; N_z^{(L)} \quad Q_y^{(L)} \quad M_{xV}^{(L)} \quad M_{x\theta}^{(L)} \right\rangle \\
&\{\mathbf{P}_2\}_{8\times1} = \int_L q_y(z)\{\mathbf{Z}_v\}_{8\times1} dz
\end{aligned} \tag{43}$$

where the component stiffnesses $[\mathbf{k}_i]_{12\times12}$, $i = 1,2,...,6$ and vector $\{\mathbf{Z}_v\}_{10\times1}$ can be found in Appendix A2.3.

5 Validation and Comparisons

The purpose of this section is to validate the theory and the finite element formulations developed in the present study for the analyses of single- or multiple-span steel beams strengthened with orthotropic GFRP laminates. The deflections, stresses, and internal resultant forces of GFRP-strengthened beams predicted by the present study will be validated/compared against those of three-dimensional finite element analyses (3D FEA) conducted in ABAQUS [40] or those of experimental studies. Key observations will be also discussed through three examples conducted in the following.

5.1 Example 1: A continuous beam bonded with GFRP laminates

Description of the problem:

A continuous steel beam with two spans of $L_{span1} = 5.0\,m$ and $L_{span2} = 3.0\,m$ are strengthened with GFRP laminates, as depicted in Figure 9a-d. The steel beam section is W150x13 that has a depth of $h = 148\,mm$, a flange width of $b = 100\,mm$, a flange thickness of $t_f = 4.9\,mm$ and a web thickness of $t_w = 4.3\,mm$. Three GFRP laminates are installed to strengthen for the beam, in which GFRP laminate 1 is $4.8\,m$ long and it is bonded to the bottom flange of span 1, GFRP laminate 2 is $2.8\,m$ long and it is bonded to bottom flange of span 2, and GFRP laminate 3 is $1.6\,m$ and it is bonded to the top flange above the intermediate support. The following longitudinal dimensions are given as $L_1 = 0.1\,m$, $L_2 = 3.9\,m$, $L_3 = 0.9\,m$, $L_4 = 0.1\,m$, $L_5 = 0.1\,m$, $L_6 = 0.5\,m$, $L_7 = 2.3\,m$ and $L_8 = 0.1\,m$. Thicknesses of all GFRP laminates are assumed as $10\,mm$ and they are stacked by 16 equal-thick laminae with fiber orientation angles of 0^0. The adhesive thicknesses are 1.0 mm. The elastic modulus and Poisson ratio of steel are assumed as $200\,GPa$ and 0.3, respectively, while those of adhesive materials are $3.18\,GPa$ and 0.3 [8]. All GFRP laminae are assumed to have a longitudinal modulus of elasticity $E_{k,z} = 45.95\,GPa$, lateral and transverse moduli of elasticity $E_{k,s} = E_{k,n} = 14.56\,GPa$,

shear stiffnesses $G_{k,sn}=G_{k,zn}=4.50\,GPa$, $G_{k,sz}=5.51\,GPa$, and Poisson's ratio $\mu_{k,sn}=\mu_{k,zn}=0.25$, $\mu_{k,sz}=0.30$ (i.e., GF800). The beam is assumed to subject two transverse point loads P and ηP, where $P=20\,kN$ and $\eta=1$, statically applied in the middles of spans 1 and 2. In this example, deflections and stresses predicted by the present study are validated against those of the 3D FEA solutions.

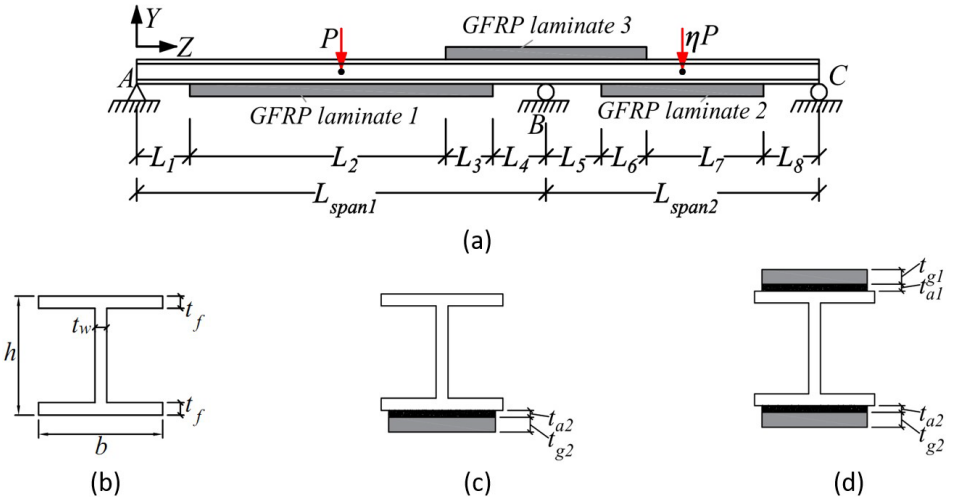

Figure 9 A two-span steel beam strengthened with GFRP laminates (a) beam profile, and cross-sections of steel segments (b) not strengthened, (c) strengthened with a bottom GFRP laminate, and (d) strengthened with two GFRP laminates

Description of the finite element modelling in the 3D FEA solution:

The finite element model is built by using C3D8R brick elements in ABAQUS library. The element has 8 nodes with 3 nodal displacements per node and it has an integration point at its center. Reduced integrations are used to avoid volumetric locking. In order to mesh the three dimensional configuration of the present GFRP-strengthened beam, 15 independent numbers of elements n_i, $i=1,2,...,15$, are proposed (Figure 10). Of which, n_1, n_2, n_3, n_4, n_6, n_7, n_8 are respectively the number of elements across the overhang part of the flanges, that across the bottom GFRP laminate thickness, that across the bottom adhesive layer thickness, that across the flange thicknesses, that along the clear web height, that across the web thickness, that across the top adhesive layer thickness and that across the top GFRP laminate thickness (Figure 10a). n_9, n_{10}, n_{11}, n_{12}, n_{13}, n_{14} and n_{15} are respectively the numbers of elements along lengths L_1, L_2, L_3, L_4+L_5, L_6, L_7 and L_8 (Figure 9a, Figure 10b). Elements of two different materials share the same nodes at interface (Figure 10a). To avoid stress localizations, loads P and ηP are converted to shear tractions applied at the web cross-sections of the steel beam.

A mesh study is conducted to investigate the convergence of the deflections and stresses in the present 3D FEA solution. Four different meshes are proposed in Table 1 and they are denoted as Meshes 1, 2, 3, and 4. Figure 11a-c present the elevation deformation view captured in ABAQUS, the beam deflection and the longitudinal normal stresses at the top fiber of the steel cross-section, respectively. As observed, the deflections are insensitive, while the stresses are slightly sensitive to the meshes. For example, the compression stresses at the location of load P based on Mesh 1 is 183.8 MPa, that based on Mesh 2 is 188.0 MPa, that based on Mesh 3 is 197.2 and that based on Mesh 4 is 197.4. When compared to the stress based on Mesh 4, the stress based on Mesh 1 is 6.9% lower, that based on Mesh 2 is 4.8% lower, while that based on Mesh 3 is only 0.1%. This indicates that the stresses of Mesh 3 are almost converged. Based on the results of the mesh study, Mesh 3 is selected for the mesh of the present 3D FEA solution. The time per run based on Mesh 3 takes about 45 minutes based on a computer with Intel(R) and Core(TM) i7-8700 processors at 3.2 and 3.19 GHz and an installed memory RAM of 16 GB.

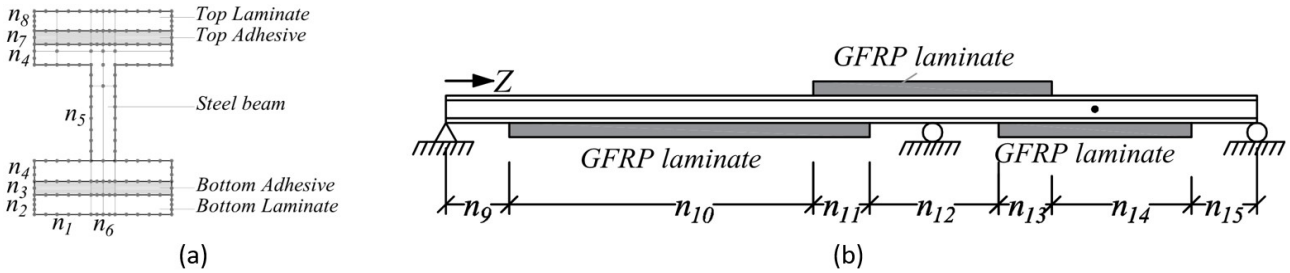

Figure 10 Independent numbers of elements for meshing of the 3D FEA model in ABAQUS (a) cross-section view, (b) elevation view

Table 1 Meshes adopted to study the result convergences in the 3D FEA solution

Mesh	n_1	n_2	n_3	n_4	n_5	n_6	n_7	n_8	n_9	n_{10}	n_{11}	n_{12}	n_{13}	n_{14}	n_{15}
1	4	4	2	2	20	2	2	4	4	39	9	8	5	23	4
2	10	8	4	4	40	4	4	8	10	156	36	20	20	92	10
3	10	16	4	4	40	4	4	16	10	312	72	20	40	184	10
4	10	16	4	4	40	4	4	16	10	624	144	20	80	368	10

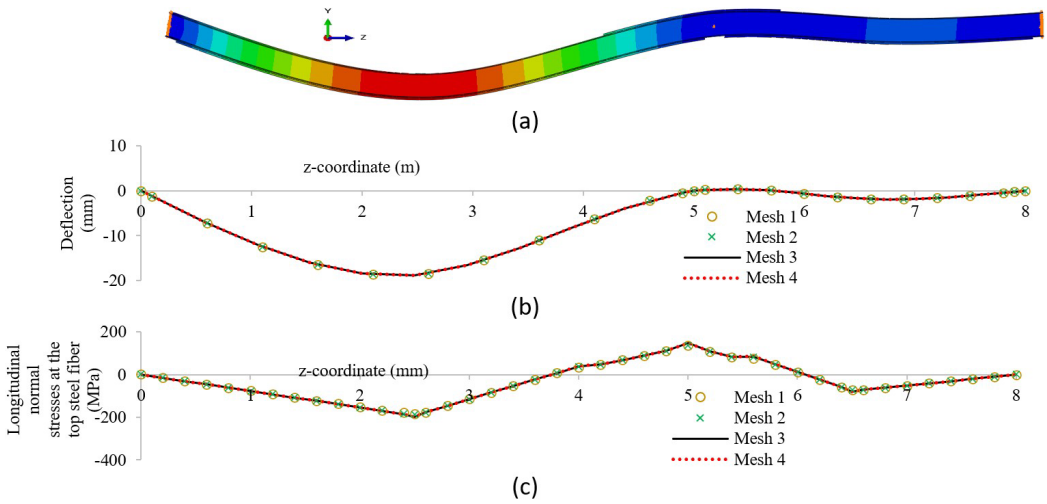

Figure 11 Deflections and stresses predicted by the 3D FEA solution in ABAQUS based on 4 different meshes (a) elevation deformation view in ABAQUS, (b) beam deflection and (c) longitudinal normal stresses at the top fiber of the steel cross-section

Description of the present finite element solution:

A mesh study for the convergence of deflections and stresses of the finite element formulations developed in the present study (i.e., Eqs. (37), (38), (40) and (42)) is also conducted. It is recalled that the present finite element formulations are based on beam elements. In order to mesh the present GFRP-strengthened beam, only 7 independent numbers of elements n_i, $i=1,2,...,7$, along lengths L_1, L_2, L_3, L_4+L_5, L_6, L_7 and L_8 are proposed. Four different Meshes 1, 2, 3, and 4 are proposed in Table 2 for the present mesh study. As observed, the deflections are converted based on all meshes, while the stresses are considered to convert by using Mesh 3 or Mesh 4 (Figure 12a,b). Based on the results of the mesh study, Mesh 3 is selected for the mesh of the present solution. The time per run based on Mesh 3 spent about 30 seconds based on the same computer as used for the run of the 3D FEA solution.

Table 2 Meshes adopted to study the result convergences in the present finite element formulations

Mesh	n_1	n_2	n_3	n_4	n_5	n_6	n_7
1	2	39	2	2	2	23	2
2	10	39	10	10	10	23	10
3	20	390	100	20	100	230	20
4	40	390	200	40	200	230	40

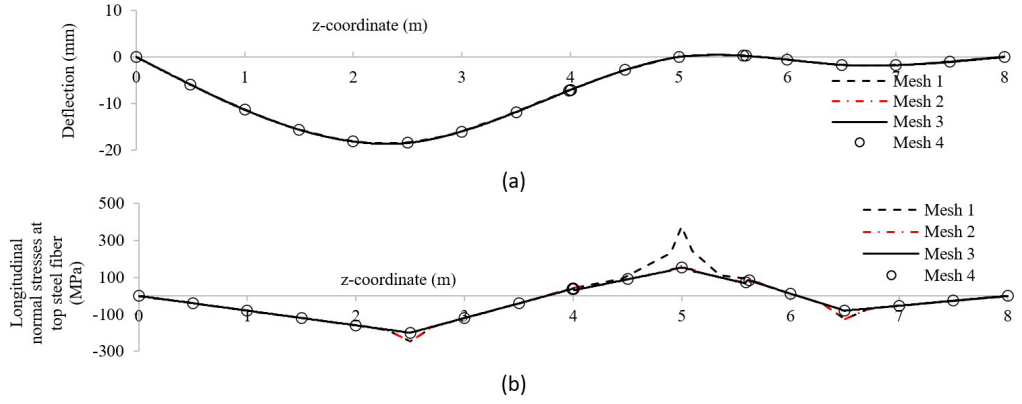

Figure 12 Deflections and stresses predicted by the present finite element formulations based on 4 different meshes (a) beam deflection and (b) longitudinal normal stresses at the top fiber of the steel cross-section

Validations and result discussions:

The comparisons of deflections and stresses as predicted by the present study and those predicted by the 3D FEA solution are presented in Figure 13a-i. As observed, the results obtained by both solutions are in excellent agreements. For example of displacements (Figure 13a), the maximum displacement at the middle span of span 1 predicted by the present study is 18.7 mm, while that predicted by the 3D FEA solution is 18.8 mm, corresponding to a difference of only 0.5%. For the longitudinal normal stresses at the top fiber of the steel cross-section (Figure 13b), the maximum stresses in magnitude are observed to occur at the middle of span 1. The stress predicted by the present study is 199.7 MPa, while that predicted by the 3D FEA solution is 197.2 MPa, corresponding to a difference of 1.3%. For the longitudinal normal stresses at the bottom fiber of the steel cross-section (Figure 13c), the maximum stresses in magnitude are observed to occur at the intermediate support (i.e., at the right end of span 1). The stress as predicted by the present study is 200.6 MPa, while that predicted by the 3D FEA solution is 198.3 MPa, corresponding to a difference of 1.2%. It is obseverd that the stresses may experience different slopes because there are changes of load, boundary and strengthening conditions. Similar observations can be obtained for the longitudinal normal stresses in the top and bottom fibers of GFRP laminate 1 (Figure 13d,f), those of GFRP laminate 2 (Figure 13e,g) and those of GFRP laminate 3 (Figure 13h,i). The positive or negative signs of the GFRP stresses are similar to those of the steel fibers where the GFRP laminates are installed.

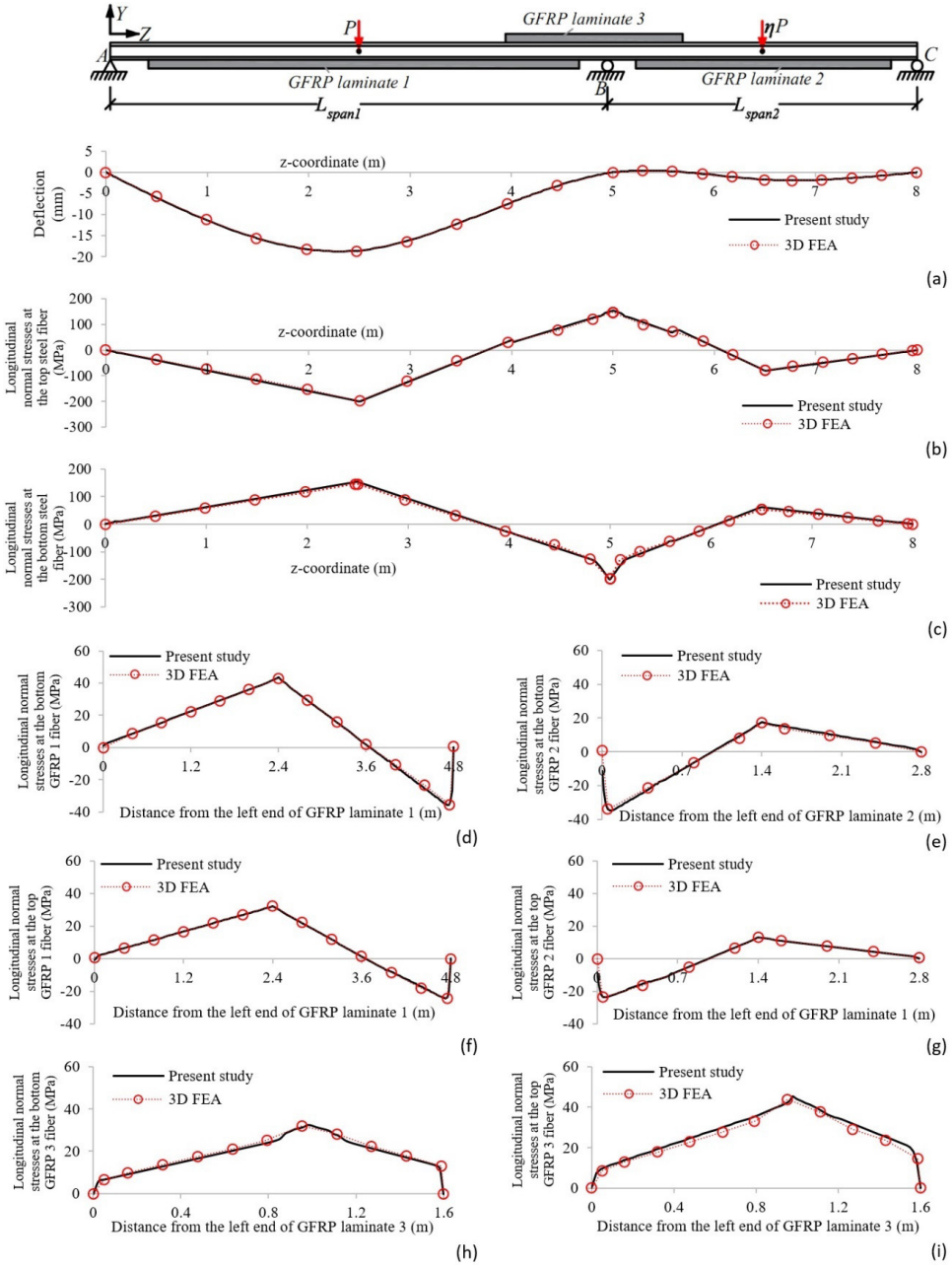

Figure 13 Comparison of the deflection and stresses results in the steel beams and the GFRP laminates between the present solution and the 3D FEA solution

Effectiveness of GFRP strengthening:

Based on the finite element formulation developed in Eq. (42) for bare steel beams (without GFRP strengthening) in the present study, the deflections and stresses of the bare beam in the present example can be evaluated. Under identical loading and boundary conditions, Figure 14a presents a comparison of the beam deflections of the bare beam and the given GFRP-strengthened beam. A significant difference between two scenarios can be obtained from the figure. For example, the deflection at the middle of span 1 in the GFRP-strengthened beam is 18.7 mm, while that in the bare beam is 23.3 mm. As a result, the effectiveness of the GFRP strengthening for the deflection is 24.6%. This is relatively suitable with the observation in an experimental study of El Damatty et al. [2]. For stresses (Figure 14b,c), the strengthening effectiveness is mostly observed at the steel fibers where the GFRP laminates are bonded with. For example of the tension stresses at the bottom fiber at the middle of the span 1 (Figure 14c), the stress of the GFRP-strengthened beam is 152.9 MPa, while that of the bare beam is 211.7 MPa, corresponding to a strengthening effectiveness of 27.8%. For the tension stresses at the top fiber at the right end of span 1 (on the intermediate support, Figure 14b), the stress based on the GFRP-strengthened beam is 153.7 MPa, while that of the bare beam is 196.7 MPa, corresponding to a strengthening effectiveness of 21.9%.

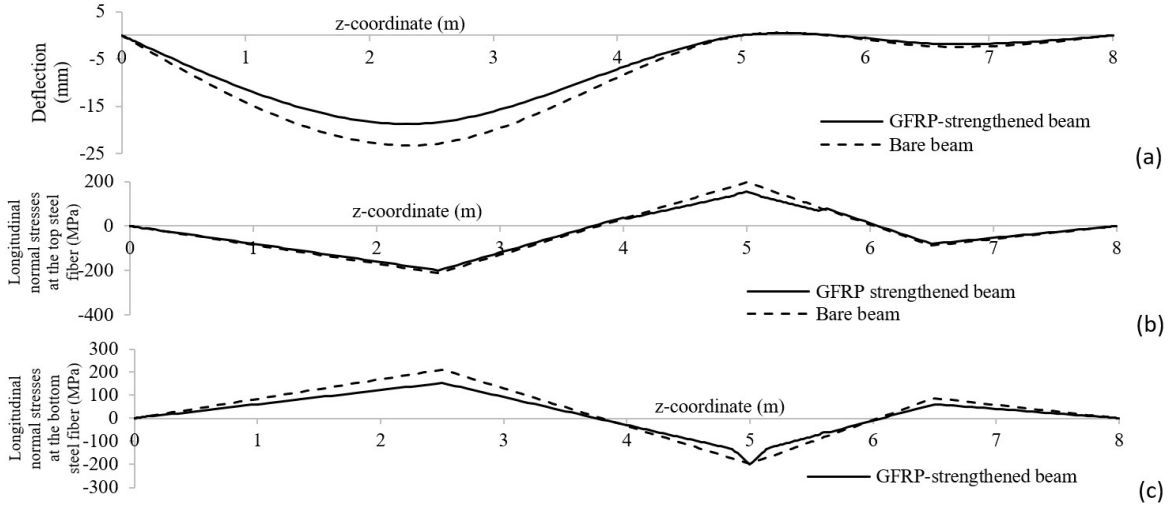

Figure 14 Effectiveness of the strengthening for the system deflections

5.2 Example 2: Validation of present solution against experimental results

Description of the problem:

El Damatty et al. (2003) conducted an experimental study for the strengthening of steel beams with W150x37 cross-sections by using GFRP laminates bonded to the top and bottom beam flanges (Figure 15a,b), in which $L_r = 2.4\,m$ and $a = 0.2\,m$. The steel section had dimensions of $h = 162\,mm$, $b = 154\,mm$, $t_f = 11.6\,mm$ and $t_w = 8.1\,mm$. The thicknesses of both GFRP laminates were $19\,mm$, while those of adhesive layers were $0.79\,mm$. Steel had an elastic modulus of $200\,GPa$ and a Poisson ratio of 0.3. GFRP laminates was reported to have a longitudinal modulus of elasticity of $17.2\,GPa$. The GFRP orthotropic lamina properties and stacking sequences were not provided. The averaged shear modulus of adhesive layer was taken as about $0.4\,GPa$. The beam is subjected to two point loads $P = 75\,kN$ applied at the locations of $L_b \approx 0.93\,mm$.

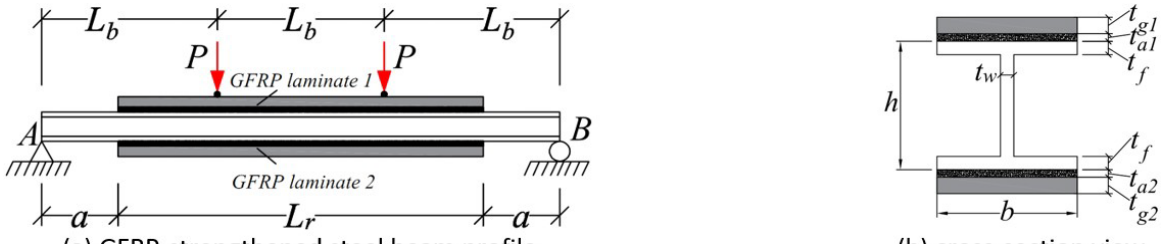

(a) GFRP-strengthened steel beam profile (b) cross-section view

Figure 15 Simply supported steel beam strengthened with two GFRP laminate subjected to point loads (El Damatty et al. 2003)

Validations of the system responses of the present solution against those of the experiment study:

A mesh study is conducted for the present finite element formulations (i.e., Eqs. (37), (42)) in a similar way as done in Example 1 to obtain converged deflections and stresses. Table 3 presents comparisons of the midspan deflections and longitudinal normal stresses as obtained from the present study and those from the experimental study by El Damatty et al. (2003). The deflection in the experimental study is 12.0mm, while that predicted by the present study is 11.9 mm, corresponding to a difference of only 0.8%. Similar observations are obtained for the longitudinal normal stresses at the bottom fiber of the steel cross-section and those at the GFRP laminate 2 (Table 3). Those indicate that the system responses predicted by the present study are in excellent agreements with the experiment results.

Table 3 Comparison of system responses of the present study against those of the experimental study

Responses	Experimental study by El Damatty et al. (2003)	Present study	% difference
Midspan deflection, (mm)	12.0	11.9	0.8
Longitudinal normal stresses at the bottom fiber of steel cross-section at midspan, (MPa)	220.0	220.8	0.4
Longitudinal normal stresses at the bottom fiber of GFRP laminate 2 at midspan, (MPa)	23.0	23.4	0.9

5.3 Example 3: GFRP-strengthened beams under the effect of GFRP laminate properties

A simply supported steel beam with a cross-section of W150x13 (i.e., $h=148mm$, $b=100mm$, $t_f=4.9mm$, and $t_w=4.3mm$) strengthened with a GFRP laminate and subjected to a uniformly distributed load $q=10\,kN/m$ is considered (Figure 16). The strengthened length L_r is $3.0m$, and the non-strengthened lengths a are $0.5m$, thus a steel span length is $L=L_r+2a=4.0\,m$. Thickness t_{g2} of the GFRP laminate is 10 mm and thickness t_{a2} of the adhesive layer is 1.0mm. The modulus of elasticity and Poisson ratio of the steel are 200 GPa and 0.3, respectively. While those of the adhesive layer are 3.18 GPa and 0.3. It is assumed that the beam is strengthened with 5 different scenarios of GFRP laminates (Table 4), of which the GFRP laminate is treated as an isotropic material in Scenario 1, that as an orthotropic material stacked by 16 laminae with stacking angles of 0^0 in Scenario 2, that as an orthotropic material stacked by 16 laminae with stacking angles of 45^0/-45^0 in Scenario 3, and that as an orthotropic material stacked by 16 laminae with stacking angles of 90^0 in Scenario 4. In Scenario 5, GFRP laminate is not strengthened for the steel beam (i.e., bare steel beam). Deflections, longitudinal normal stresses in steel and axial resultant forces in the GFRP laminate will be predicted by the present solutions and they are validated against 3D FEA solutions in ABAQUS. The effect of the orthotropic and stacking properties of the GFRP laminates on such system responses will be clarified.

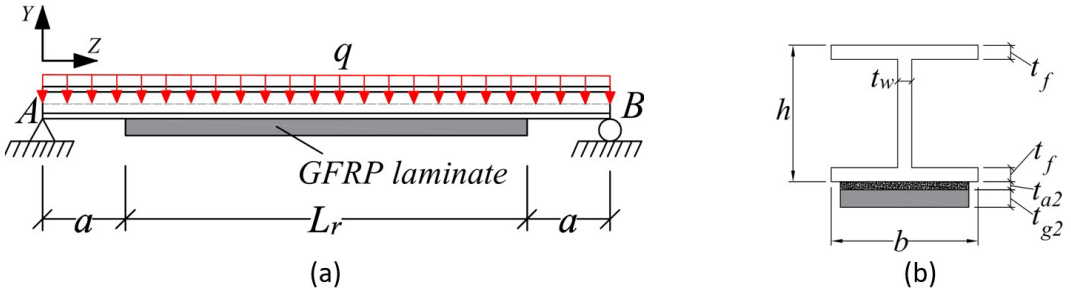

Figure 16 A steel beam strengthened with a bottom GFRP laminate subjected to uniformly distributed loads

Validations and result discussions:

Figure 17 presents a comparison of the beam deflections as predicted by the present study and the 3D FEA solution under different Scenarios 1-5 of the GFRP laminates. Table 5 summarizes the comparison of the midspan deflections. For each Scenario, the deflection curve predicted by the present study is observed to excellently agree with that predicted by the 3D FEA solution. For example of Scenario 2 (with lamina stacking angles of 0^0), the midspan deflection based on the present study is 23.5 mm, that based on the 3D FEA solution is 23.6 mm, corresponding to a difference of only 0.4%. In Scenario 3 (with lamina stacking angles of 45^0/-45^0), the midspan deflection predicted by the present study is 25.6 mm, while that predicted by the 3D FEA solution is 25.8 mm, a difference of 0.8%. The midspan deflection in Scenario 4 based on the present solution and that based on the 3D FEA solution are not different and they are equal to 26.5 mm.

The effect of the GFRP laminate properties on the beam deflection can be observed in Figure 17 and Table 5. The midspan deflection based on Scenario 1 (i.e., isotropic GFRP laminate) is the lowest one (i.e., 23.45mm), and it increases to 23.5 mm in Scenario 2 (laminae with stacking angles of 0^0), 25.6mm in Scenario 3 (laminae with stacking angles of 45^0/-45^0), and 26.5 mm in Scenario 4 (laminae with stacking angles of 90^0). Therefore, it here observes that the increase of fiber stacking angles (from 0^0 to 90^0) of the GFRP laminate may lead to the increase of the beam deflections. In the present study, it is observed that when the stacking angles increase, they decrease axial and transversely flexural stiffnesses $\overline{A}_{gi,11}$, $\overline{D}_{gi,11}$ (as defined in Eqs. (18)) of the GFRP laminate. Specifically, the values of $\overline{A}_{gi,11}$ and $\overline{D}_{gi,11}$ for Scenario 2 with stacking angles of 0^0 are evaluated as $4.6\times10^5\ N/mm$ and $3.8\times10^6\ N.mm$, while those for Scenario 3 with stacking angles of 45^0/-45^0 are $1.7\times10^5\ N/mm$ and $1.4\times10^6\ N.mm$, and those for Scenario 4 with stacking angles of 90^0 are $1.4\times10^5\ N/mm$ and $1.2\times10^6\ N.mm$. Such an axial-transversely flexural response is different to a lateral-torsional response of the composite beams. (i..e., the GFRP laminates stacked by laminae with 45^0/-45^0 stacking angles often generate a maximum effectiveness for the system responses in lateral-torsional analyses (Lee and Lee 2004, Phe 2022)).

Table 4 Different scenarios of GFRP laminate properties in Example 3

Scenario	Behavior	Number of laminae	Lamina thickness	Lamina properties*					Lamina stacking angles
				$E_{k,z}$	$E_{k,s}$	$G_{k,sz}$	$v_{k,zs}$	$v_{k,sz}$	
1	Isotropic	N.A.	N.A.	45.95	45.95	17.67	0.3	0.3	N.A.
2									$(0/0/0/0/0/0/0/0)_s$
3	Orthotropic	16	0.625	45.95	14.56	5.51	0.3	0.095	$(45/-45/45/-45/45/-45/45/-45)_s$
4									$(90/90/90/90/90/90/90/90)_s$
5	No GFRP strengthening								

* units of $E_{k,z}$, $E_{k,s}$ and $G_{k,sz}$ are GPa.

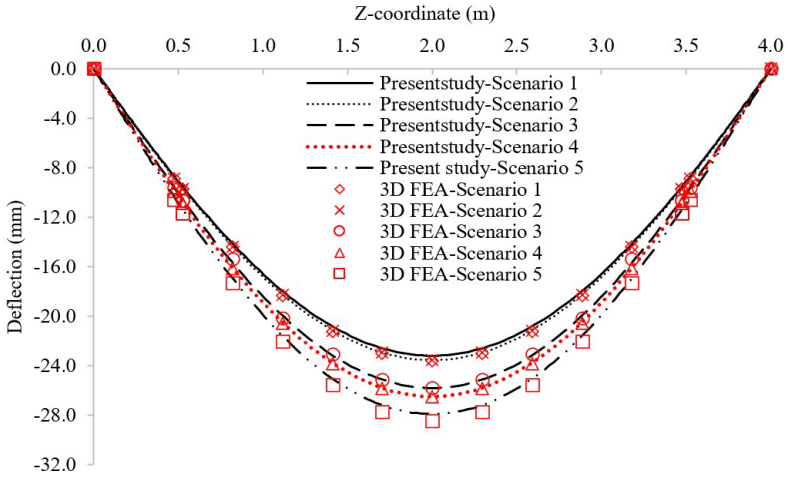

Figure 17 Comparison of the beam deflections between the present study and the 3D FEA solution under different Scenarios 1-5 of the GFRP laminates

Based on Table 5, it is observed that the effectiveness of GFRP strengthening also depends on the fiber stacking angles of the GFRP laminates. For example, by comparing the deflection in Scenario 2 (i.e., 23.5 mm) against that in Scenario 5 (i.e., 28.1 mm, no GFRP strengthening), an effectiveness of 16.4% is observed. However, by comparing the deflection in Scenario 3 (i.e., 25.6 mm) against that in Scenario 5, the effectiveness is only 8.9%.

Figure 18a present comparisons of the longitudinal normal stresses at the bottom fiber of the steel cross-section in Scenario 2, as predicted by the present study and the 3D FEA solutions. While Figure 18b present comparisons of the stresses in Scenario 3, as predicted by the present study and the 3D FEA solutions. Also, Figure 19a-b present comparisons of the axial (internal) resultant forces in the GFRP laminate (i.e., N_{z2} in Eq. (35)) in Sceneries 2 and 3, as predicted by the present study and the 3D FEA solutions. For both Scenarios, the normal stresses and the resultant forces predicted by the present study are observed to excellently agree with those predicted by the 3D FEA solution. For example, the normal stresses at midspan in Figure 18a predicted by the present study is 173.3 MPa, that predicted by the 3D FEA solution is 174.3 MPa, corresponding to a difference of only 0.6%. In Figure 19b, the resultant force at midspan predicted by the present study and the 3D FEA solutions are 19.5 kN and 19.4 kN, respectively, a difference of only 0.5%.

The effect of the GFRP lamina stacking angles on the normal stresses and internal resultant forces can be also observed in Figure 18a-b and Figure 19a-b. The peak normal stresses predicted by the present solution based on Scenario 2 (Figure 18a) is 173.3 MPa, while that based on Scenario 3 is 220 MPa, a difference of 27.0%. Also, the peak internal resultant forces in GFRP laminates predicted by the present solution in Scenario 2 (Figure 18a) is 44.3 kN, that in Scenario 3 is 19.5 MPa, a difference of 56.0%. It is recalled that the GFRP lamina stacking angles is 0^0 in Scenario 2 while that is 45^0/-45^0 in Scenario 3 (as defined in Table 4). Therefore, it is here observed that the increase of lamina stacking angles of the GFRP laminates may cause an increase of the longitudinal normal stresses in the steel beam and a decrease of the axial resultant force in the GFRP laminate, that leads to a lower strengthening effectiveness.

Table 5 Comparison of the midspan deflection (mm) between the present study and 3D FEA solution under different Scenarios 1-5 of the GFRP laminate

Scenario	Present study*	3D FEA solution*	% difference
1	23.45	23.6	0.6
2	23.5	23.6	0.4
3	25.6	25.8	0.8
4	26.5	26.5	0.0
5	28.1	28.5	1.4

* Negative signs of deflections are converted to positive ones

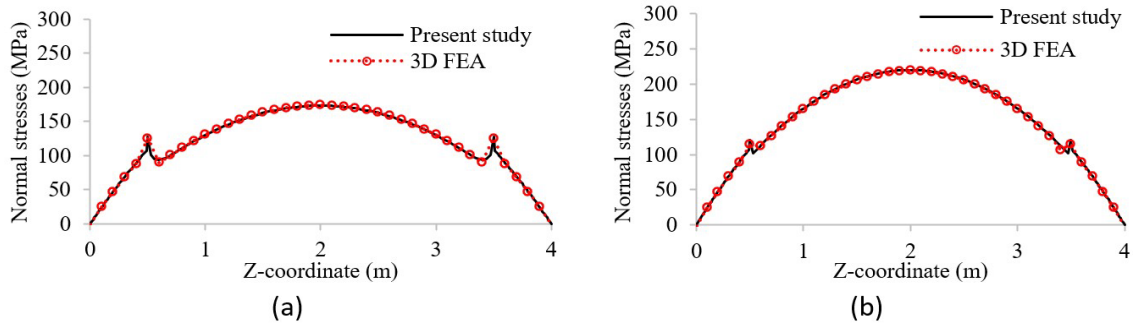

Figure 18 Comparison of the longitudinal normal stresses at the bottom fiber of steel in (a) Scenario 2 and (b) Scenario 3 as predicted by the present study and the 3D FEA solution

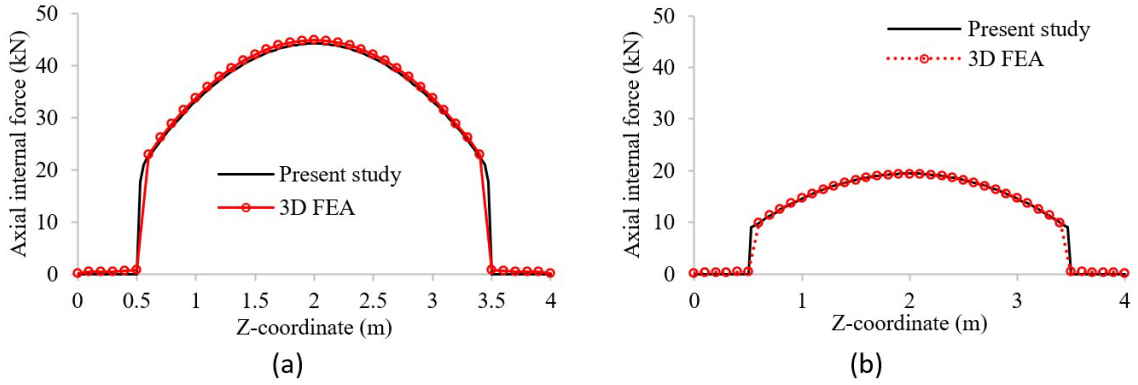

Figure 19 Comparison of the internal resultant forces in the GFRP laminate in (a) Scenario 2 and (b) Scenario 3, as predicted by the present study and the 3D FEA solution

6 Parametric studies

The present parametric study is conducted to further investigate the effect of GFRP laminate properties on the deflections of GFRP-strengthened steel beams. The given structures in Scenarios 2 and 3 of Example 3 are re-considered and they are taken as reference cases. Based on the present FE solution, the GFRP lamina properties $E_{k,z}$, $E_{k,s}$, $G_{k,sz}$ and the GFRP laminate thickness t_{g2} are separately varied to investigate their effects on the midspan deflection. Specifically, $E_{k,z}$ is varied from 9.0 GPa to 92 GPa, $E_{k,s}$ is varied from 2.9 GPa to 46 GPa, $G_{k,sz}$ is varied from 0 GPa to 17.7 GPa, and t_{g2} is varied from 2.0 mm to 30 mm. When one parameter is varied, other properties are kept unchanged as given in the reference cases.

Figure 20a-d respectively present the effects of the longitudinal lamina modulus $E_{k,z}$, the lateral lamina modulus $E_{k,s}$, the lamina shear modulus $G_{k,sz}$, and the laminate thickness t_{g2} on the midspan deflection in Scenario 2 (i.e., a GFRP laminate is stacked by GFRP laminae with 0^0 stacking angles). As observed, the system deflection is sensitive to $E_{k,z}$ and t_{g2} while it is insensitive to $E_{k,s}$ and $G_{k,sz}$. This can explained through plate stiffnesses $\overline{A}_{gi,11}, \overline{D}_{gi,11}$ in Scenario 2, those are dependent on $E_{k,z}$ and t_{g2} but independent on $E_{k,s}$ and $G_{k,sz}$, as proved in Eqs. (A.5) of Appendix 1.

Figure 21a-d respectively present the effects of the longitudinal lamina modulus $E_{k,z}$, the lateral lamina modulus $E_{k,s}$, the lamina shear modulus $G_{k,sz}$, and the laminate thickness t_{g2} on the midspan deflection in Scenario 3 (i.e., a GFRP laminate is stacked by GFRP laminae with 45^0/-45^0 stacking angles). It is observed that the system deflection is slightly dependent on $E_{k,z}$ and $E_{k,s}$, while it strongly depends of $G_{k,sz}$ and t_{g2}. Again, this can be explained through plate stiffnesses $\overline{A}_{gi,11}, \overline{D}_{gi,11}$ in Scenario 3. As proved in Eqs. (A.6) of Appendix 1, stiffnesses $\overline{A}_{gi,11}, \overline{D}_{gi,11}$ are evaluated through all four parameters $E_{k,z}$, $E_{k,s}$, $G_{k,sz}$ and t_{g2}, in which $G_{k,sz}$ and t_{g2} mostly contribute to the magnitudes of $\overline{A}_{gi,11}, \overline{D}_{gi,11}$.

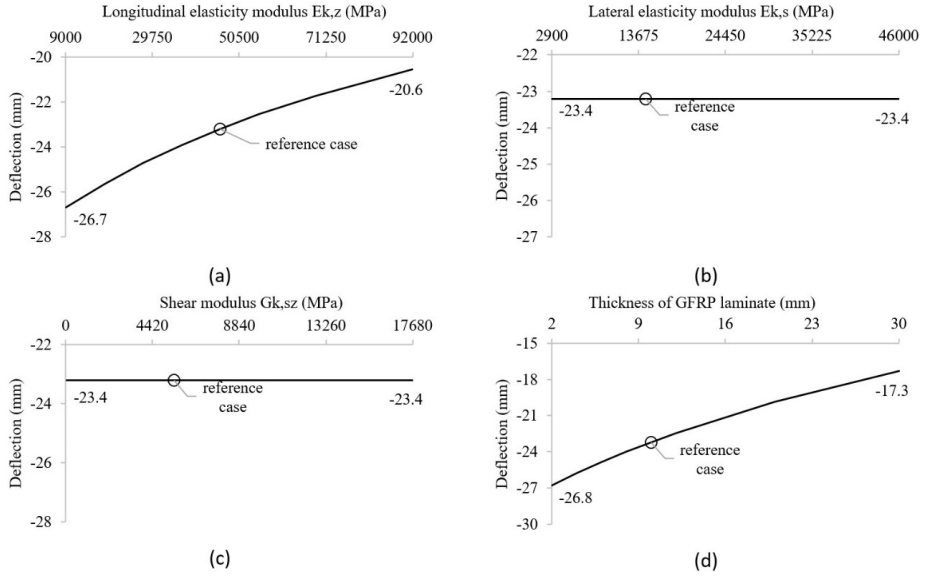

Figure 20 Effect of the GFRP properties on midspan deflection in Scenario 2, (a) longitudinal lamina modulus $E_{k,z}$, (b) lateral lamina modulus $E_{k,s}$, (c) Lamina shear modulus $G_{k,sz}$, and (d) laminate thickness t_{g2}

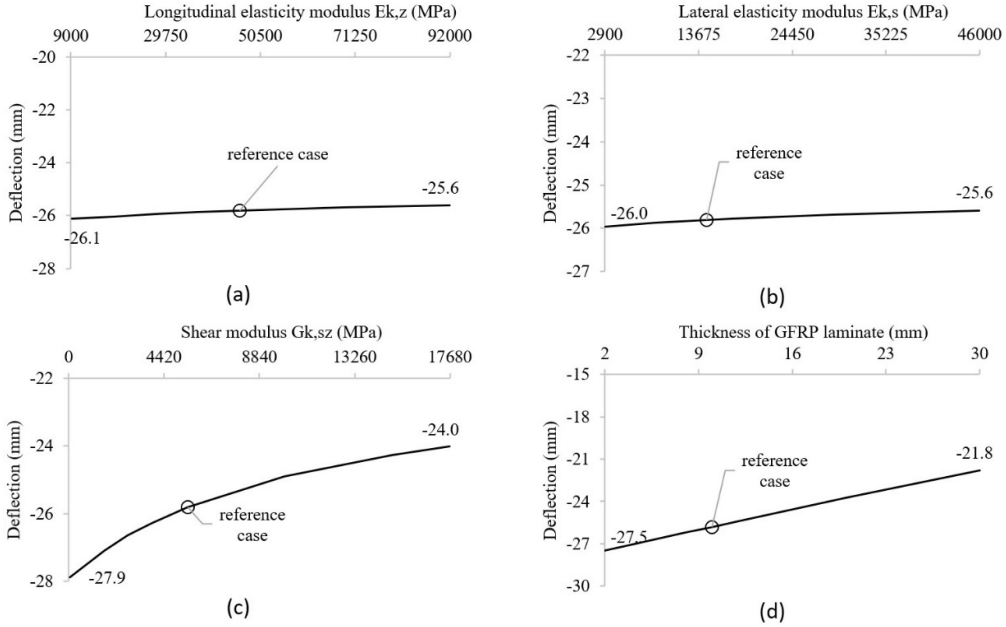

Figure 21 Effect of the GFRP properties on midspan deflection in Scenario 3, (a) longitudinal lamina modulus $E_{k,z}$, (b) lateral lamina modulus $E_{k,s}$, (c) Lamina shear modulus $G_{k,sz}$, and (d) laminate thickness t_{g2}

7 Conclusions

The present study has successfully developed an innovated shear deformable theory and four finite element (FE) formulations based on the first variational principle of stationary potential energy for the analysis of steel beams strengthened with orthotropic GFRP laminates under transverse loadings. The FE formulations were developed by using linear and cubic shape functions. The present study captured orthotropic properties of the GFRP laminae, GFRP lamina stacking sequences, partial interaction between the steel beam and the GFRP laminates, and shear deformations. Based on the validations and comparisons presented in three examples and two parameter studies, important conclusions were achieved in the present study and they are summarized in the following.

1. The FE formulations developed in the present study were based on beam elements. The system responses (i.e., deflections, stresses, and internal resultant forces) predicted by the present FE solutions were successfully validated against those of experimental studies and/or three-dimensional finite element analyses (3D FEA). Meanwhile, the running time of an analysis based on the present FE solution was orders of magnitude lower than that based on the 3D FEA solution, as discussed in Examples 1 and 2.
2. The system responses of GFRP-strengthened beams were significantly influenced by GFRP fiber angle arrangements of GFRP laminates. As discussed in Example 3 and parametric studies, GFRP laminates with fiber orientation angles of 0 degrees maximized the axial and transversely flexural laminate stiffnesses and thus minimized the responses of the strengthened steel beams.
3. For steel beams strengthened with GFRP laminates stacked by GFRP laminae with 0^0 stacking angles, their deflections are strongly influenced by the longitudinal GFRP lamina modulus and the GFRP laminate thickness, while they are insensitive to the lateral GFRP lamina modulus and the GFRP lamina shear modulus. However, for steel beams strengthened with GFRP laminate stacked by GFRP laminae with 45^0/-45^0 stacking angles, their deflections are strongly influenced by the GFRP shear modulus and the GFRP laminate thickness, while they are slightly influenced by longitudinal GFRP lamina modulus and the lateral GFRP lamina modulus, as observed in the parametric studies.
4. The effectiveness of GFRP strengthening for both single and continuous steel beams were quantified in present study. For example of Example 1, the effectiveness for the beam deflection was 24.6%, that for tension stresses at the bottom steel fiber at the middle of the first span was 21.9%, and that for tension stresses at the top steel fiber at the right end of the first span was 27.8%.
5. The present finite element formulations are applicable to single or multiple span GFRP-strengthened beams subjected to various loading and boundary conditions. However, they can only predict the linearly elastic responses including stresses, deflections, and internal resultant forces of the system. Hence, they are applicable to check several system failure modes, such as moment resistance based on steel yielding, GFRP stress control, and deflection. Also, they can predict pre-buckling internal resultant forces those maybe necessary for a further lateral-torsional buckling analysis.

Acknowledgements

This research is funded by University of Transport and Communications (UTC) under grant number T2022-CT-007TD.

Author's Contribuitions: Conceptualization, PV Phe and BT Thanh, Methodology, PV Phe and BT Thanh, Investigation, PV Phe, Writing-original draft, PV Phe and BT Thanh, Writing - review & editing Phe PV, Funding acquisition, PV Phe and BT Thanh, Resources, PV Phe and BT Thanh.

Editor: Marco L. Bittencourt

References

Accord, E., and Earls, C.J. (2006). Use of fiber-reinforced polymer composite elements to enhance structural steel member ductility. J. of composites for construction ASCE 10: 337-344.

Aguilera, J. and Fam, A. (2013). Bonded FRP Plates for Strengthening Rectangular Hollow Steel Section T-Joints against Web Buckling Induced by Transverse Compression. J. of Composites for Construction, ASCE, 17(4): 421-432.

Ali, H., Assih, J., and Li, A. (2021). Flexural capacity of continuous reinforced concrete beams strengthened or repaired by CFRP/GFRP sheets. Int. J. of Adhesion and Adhesives 104: 102759.

Andrade, A., Barroso, V.S., Providencia, P., and Challamel, N. (2023). A linear two-dimensional mathematical model for thin two-layer plates with partial shear interaction, with a view towards application to laminated glass. Thin Walled Structures 182: 110255.

Asta, D. A. (2001). Composite beams with weak shear connection. Int. J. of Solids and Structures 38(32-33): 5605-5624.

Aydin E, and Aktas M. (2015). Obtaining a permanent repair by using GFRP in steel plates reformed by heat-treatment. Thin-Walled Structures 94: 13–22.

Back, S.Y., and Will, K.M. (2008). Shear-flexible thin-walled element for composite I-beams. Engineering Str. 30(5): 1447–1458.

Challamel, N., Bernard, F. and Casandjian, C. (2010). Out-of-plane behavior of partially composite or sandwich beams by exact and finite element methods. Thin-Walled Structures 48(8): 561-580.

Challamel, N. and Girhammar, U.A. (2012). Lateral-torsional buckling of vertically layered composite beams with interlayer slip under uniform moment. Engineering Structures 34(46): 505-513.

Correia, J. R., Branco, F. A., Silva, N. M. F., Camotim, D., and Silvestre, N. (2011). First-order, buckling and post-buckling behavior of GFRP pultruded beams. Part 1: Experimental study. Computers & Structures 89(21-22): 2052-2064.

Ditaranto, R.A. (1973). Static analysis of a laminated beam. J. of Manufacturing Science and Engineering 95(3): 755-761.

El Damatty, A.A. and Abushagur, M. (2003). Testing and modeling of shear and peel behavior for bonded steel/FRP connections. Thin-Walled Structures 41(11): 987-1003.

El Damatty, A., Abushagur, M. and Youssef, M. A. (2003). Experimental and analytical investigation of steel beams rehabilitated using GFRP sheets. Journal of Steel and Composite Structures 3(6): 421-438.

Gara, F., Ranzi, G. and Leoni, G. (2006).Displacement-based formulations for composite beams with longitudinal slip and vertical uplift. Int. J. for Numerical Methods in Engineering 65(8): 1197-1220.

Girhammar, U.A. and Pan, D.H. (2007). Exact static analysis of partially composite beams and beam-columns. International Journal of Mechanical Sciences 49(2): 239-255.

Harries, A.K. and El-Tawil, S. (2008). Steel-FRP composite structural systems. International Conference on Composite Construction in Steel and Concrete, Composite Construction in Steel and Concrete VI, Colorado, United States, October.

Hosseini, S. A., Bahaari, M.R., Lesani, M., Hajikarimi, P. (2021). Static load-bearing capacity formulation for steel tubular T/Y-jointsstrengthened with GFRP and CFRP. Composite Structures 267: 113950.

Ibrahim S.S., Eswari, S. and Sundararajan, T. (2018). Behaviour of hybrid fibre reinforced concrete beams strengthened with GFRP laminates. Structural Engineering and Mechanics 66(5): 631-636.

Koutsawa, Y., and Daya, E.M. (2007). Static and free vibration analysis of laminated glass beam on viscoelastic supports. Int. J. of Solids & Structures 44(25-26): 8735-8750.

Koziey BL, Mirza FA. (1997). Consistent thick shell element. Computer Structures 65(12): 513–41.

Lee, J. and Lee, S.-H. (2004). Flexural-torsional behavior of thin-walled composite beams. Thin-Walled Stru. 42(9): 1293-1305.

Lesani, M., Hosseini, S. A., Bahaari, M.R. (2022). Load bearing capacity of GFRP-strengthened tubular T-joints: Experimental and numerical study. Structures 38: 1151-1164.

Maddur, S.S. and Chaturvedi, S. K. (1999). Laminated composite open profile sections: First order shear deformation theory. Composite Structures 45(2): 105-114.

Nowzartash, F. and Mohareb, M. (2005). Planar bending of sandwich beams with transverse loads off the centroidal axis. Journal of Structural Engineering 131(4): 385-396.

Parvathi, E., Lashmanan, M., Mini K. M. (2018). Strengthening Steel Members with Holes Under Tension Using Unidirectional GFRP Sheets. I. Journal of Steel Structures 18: 496–511.

Phe, P.V., and Mohareb, M.(2014). A shear deformable theory for the analysis of steel beams reinforced with GFRP plates. Journal of Thin-Walled Structures 85: 165-182.

Phe, P.V and Mohareb, M. (2015). Nonshear Deformable Theory for Analysis of Steel Beams Reinforced with GFRP Plate Closed-Form Solution. Journal of Structural Engineering ASCE 141(12): 04015063.

Phe, P.V., Mohareb, M., and Fam, A. (2017). Analysis of Steel Beams Strengthened with GFRP Plates Including Pre-existing Loading Effects. J. Structural Engineering, ASCE 143: 04017163.

Phe, P.V., Mohareb, M., and Fam, A. (2018). Lateral Torsional Buckling Analysis of Steel Beams Strengthened with GFRP plate. Journal of Thin-Walled Structures 131: 55-75.

Phe, P.V. (2021). Solutions of the interfacial shear and normal stresses in plate flexural-strengthened beams based on different complementary strain energy assumptions. Engineering Structures 229: 111567.

Phe, P.V. (2022). An innovated theory and closed form solutions for the elastic lateral torsional buckling analysis of steel beams/columns strengthened with symmetrically balanced GFRP laminates. Engineering Structures 256: 114046.

Raj, F. M., Nagarajan, V.A., Elsi, S. S., Jayaram, R.S. (2016). Effect of fiber content on flexural properties of fishnet/GFRP hybrid composites. Steel and Composite Structures 22(1): 13-24.

Sun, Q., Zhang, N., and Liu, X. (2022), “A numerically stable exact method for analysis of partial-interaction composite beams based on Timoshenko beam theory”, Eng. Structures, 273, 115049.

Smith, S.T., and Teng, J.G. (2001). Interfacial stresses in plated beams, Engineering Structures 23: 857-871.

Ranzi, G., and Zona, A. (2007). A steel–concrete composite beam model with partial interaction including the shear deformability of the steel component. Engineering Structures 29: 3026–3041.

Youssef M. (2006). Analytical prediction of the linear and nonlinear behaviour of steel beams rehabilitated using FRP sheets. Engineering Structures 28:903–911.

Siddique M.A.A., El Damatty A.A. (2012). Enhancement of buckling capacity of steel plates strengthened with GFRP plates. Thin-Walled Structures, 60:154–62.

Siddique M.A.A., El Damatty A.A. (2013). Improvement of local buckling behaviour of steel beams through bonding GFRP plates. Composite Structures, 96:44 56.

Zaghian S, Mohareb M. (2019). Elastic buckling strength for steel plates symmetrically Strengthened with glass fiber reinforced polymer plates, Canadian Journal of Civil Engineering, 47: 337-353.

Appendix 1. Evaluation of the GFRP laminate stiffnesses

Plane stress-reduced stiffnesses of the k^{th} GFRP lamina may be evaluated as [10,39]

$$Q_{k,11}=E_{k,z}\big/\left(1-v_{zs}v_{sz}\right),\quad Q_{k,12}=v_{zs}E_{k,s}\big/\left(1-v_{zs}v_{sz}\right),\quad Q_{k,22}=E_{k,s}\big/\left(1-v_{zs}v_{sz}\right),\qquad Q_{k,66}=G_{k,sz} \tag{1.1}$$

In which parameters $E_{k,z}$, $E_{k,s}$, $G_{k,sz}$, and $v_{k,zs},\ v_{k,sz}$ have been defined in Section 3.4. Then, the transformed lamina stiffnesses can be evaluated as

$$\begin{aligned}
\bar{Q}_{k,11}&=Q_{k,11}\cos^4\gamma_k+2\left(Q_{k,12}+2Q_{k,66}\right)\sin^2\gamma_k\cos^2\gamma_k+Q_{k,22}\sin^4\gamma_k,\\
\bar{Q}_{k,12}&=\left(Q_{k,11}+Q_{k,22}-4Q_{k,66}\right)\sin^2\gamma_k\cos^2\gamma_k+Q_{k,12}\left(\sin^4\gamma_k+\cos^4\gamma_k\right),\\
\bar{Q}_{k,22}&=Q_{k,11}\sin^4\gamma_k+2\left(Q_{k,12}+2Q_{k,66}\right)\sin^2\gamma_k\cos^2\gamma_k+Q_{k,22}\cos^4\gamma_k,\\
\bar{Q}_{k,16}&=\left(Q_{k,11}-Q_{k,12}-2Q_{k,66}\right)\sin\gamma_k\cos^3\gamma_k+\left(Q_{k,12}-Q_{k,22}+2Q_{k,66}\right)\sin^3\gamma_k\cos\gamma_k,\\
\bar{Q}_{k,26}&=\left(Q_{k,11}-Q_{k,12}-2Q_{k,66}\right)\sin^3\gamma_k\cos\gamma_k+\left(Q_{k,12}-Q_{k,22}+2Q_{k,66}\right)\sin\gamma_k\cos^3\gamma_k,\\
\bar{Q}_{k,66}&=\left(Q_{k,11}+Q_{k,22}-2Q_{k,12}-2Q_{k,66}\right)\sin^2\gamma_k\cos^2\gamma_k+Q_{k,66}\left(\sin^4\gamma_k+\cos^4\gamma_k\right)
\end{aligned} \tag{1.2}$$

where γ_k is the fiber orientation angle of the k^{th} lamina. The extensional and bending stiffnesses of the GFRP laminate can be evaluated as

$$A_{gi,ej}=\sum_{k=1}^{n}\bar{Q}_{k,ej}\left(\bar{y}_{k+1}-\bar{y}_k\right),\qquad D_{gi,ej}=\sum_{k=1}^{n}\bar{Q}_{k,ej}\left(\bar{y}_{k+1}^3-\bar{y}_k^3\right)\Big/3 \tag{1.3}$$

where $e,j=1,2,...,6$. t_k is the k^{th} lamina thickness, while $\bar{y}_k^*$ is the coordinate of the middle surface of the k^{th} lamina. Based on Eqs. (A.3), plate stiffnesses $\bar{A}_{gi,11},\ \bar{D}_{gi,11}$ in Eqs. (18) can be derived as:

$$\bar{A}_{gi,11}=A_{gi,11}-A_{gi,12}^2\big/A_{gi,22},\quad \bar{D}_{gi,11}=D_{gi,11}-D_{gi,12}^2\big/D_{gi,22} \tag{1.4}$$

For GFRP laminate stacked by is 0^0 lamina angles, the plate stiffnesses can be simplified as

$$\bar{A}_{gi,11}=t_{g2}E_{k,z},\qquad \bar{D}_{gi,11}=\frac{t_{g2}^3}{12}E_{k,z} \tag{1.5}$$

While for GFRP laminate symmetrically stacked by is 45^0/-45^0 lamina angles, the plate stiffnesses can be obtained as

$$\begin{aligned}
\bar{A}_{gi,11}&=4t_{g2}G_{k,sz}\frac{\left(1+v_{sz}\right)E_{k,z}+\left(1+v_{zs}\right)E_{k,s}}{\left(1+v_{sz}\right)E_{k,z}+\left(1+v_{zs}\right)E_{k,s}+4\left(1-v_{zs}v_{sz}\right)G_{k,sz}},\\
\bar{D}_{gi,11}&=\frac{t_{g2}^3}{12}4G_{k,sz}\frac{\left(1+v_{sz}\right)E_{k,z}+\left(1+v_{zs}\right)E_{k,s}}{\left(1+v_{sz}\right)E_{k,z}+\left(1+v_{zs}\right)E_{k,s}+4\left(1-v_{zs}v_{sz}\right)G_{k,sz}}
\end{aligned} \tag{1.6}$$

For GFRP laminate stacked by is 90^0 lamina angles, the plate stiffnesses can be obtained as

$$\bar{A}_{gi,11}=t_{g2}E_{k,s},\qquad \bar{D}_{gi,11}=\frac{t_{g2}^3}{12}E_{k,s} \tag{1.7}$$

Appendix 2. Stiffness matrices of finite element formulations in Eqs. (38), (40), (42)

A2. 1 A steel beam element strengthened with a GFRP laminate bonded to the top flange (Eq. (38))

The governing displacement fields are interpolated from the nodal displacements as follows.

$$\begin{aligned} W(z)&=\left\langle \mathbf{F}_l(z)\right\rangle_{1\times 2}^T\left[\boldsymbol{\rho}_w\right]_{2\times 10}\{\boldsymbol{\Delta}\}_{10\times 1}, \qquad W_1(z)=\left\langle \mathbf{F}_l(z)\right\rangle_{1\times 2}^T\left[\boldsymbol{\rho}_{w1}\right]_{2\times 10}\{\boldsymbol{\Delta}\}_{10\times 1},\\ V(z)&=\left\langle \mathbf{F}_c(z)\right\rangle_{1\times 4}^T\left[\boldsymbol{\rho}_v\right]_{4\times 10}\{\boldsymbol{\Delta}\}_{10\times 1}, \qquad \theta_x(z)=\left\langle \mathbf{F}_l(z)\right\rangle_{1\times 2}^T\{\boldsymbol{\Delta}\}_{10\times 1}\end{aligned} \tag{2.1.1}$$

in which the index matrices are defined as

$$\begin{aligned} \left[\boldsymbol{\rho}_w\right]_{2\times 10}&=\left[\begin{array}{ccccc:ccccc}1&0&0&0&0&0&0&0&0&0\\0&0&0&0&0&1&0&0&0&0\end{array}\right], \quad \left[\boldsymbol{\rho}_{w1}\right]_{2\times 10}=\left[\begin{array}{ccccc:ccccc}0&1&0&0&0&0&0&0&0&0\\0&0&0&0&0&0&1&0&0&0\end{array}\right]\\ \left[\boldsymbol{\rho}_v\right]_{4\times 10}&=\left[\begin{array}{ccccc:ccccc}0&0&1&0&0&0&0&0&0&0\\0&0&0&1&0&0&0&0&0&0\\0&0&0&0&0&0&0&1&0&0\\0&0&0&0&0&0&0&0&1&0\end{array}\right], \quad \left[\boldsymbol{\rho}_{\theta x}\right]_{2\times 10}=\left[\begin{array}{ccccc:ccccc}0&0&0&0&1&0&0&0&0&0\\0&0&0&0&0&0&0&0&0&1\end{array}\right]\end{aligned} \tag{2.1.2}$$

and $\left\langle \mathbf{F}_l(z)\right\rangle_{1\times 2}^T, \left\langle \mathbf{F}_c(z)\right\rangle_{1\times 4}^T$ have been defined in Eq. (29). The component stiffnesses $\left[\mathbf{k}_i\right]_{12\times 12}$, $i=1,2,...,14$, defined in Eq. (38) can be determined as

$$\begin{aligned}
&\left[\mathbf{k}_1\right]=E_sA_s\left[\boldsymbol{\rho}_w\right]_{10\times 2}^T\left[\mathbf{H}_{ll,1}\right]_{2\times 2}\left[\boldsymbol{\rho}_w\right]_{2\times 10}, \qquad \left[\mathbf{k}_2\right]=E_s\left(\frac{bt_fh_b^2}{2}+\frac{t_wh_b^3}{12}\right)\left[\boldsymbol{\rho}_{\theta x}\right]_{10\times 2}^T\left[\mathbf{H}_{ll,1}\right]_{2\times 2}\left[\boldsymbol{\rho}_{\theta x}\right]_{2\times 10},\\
&\left[\mathbf{k}_3\right]=\left(E_s\frac{2bt_f^3}{12}+\bar{D}_{g1,11}b\right)\left[\boldsymbol{\rho}_v\right]_{10\times 4}^T\left[\mathbf{H}_{cc,2}\right]_{4\times 4}\left[\boldsymbol{\rho}_v\right]_{4\times 10}, \quad \left[\mathbf{k}_4\right]=\left(G_sh_wt_w+G_{a1}A_{a1}\frac{\left(2t_{a1}+t_f+t_{g1}\right)^2}{\left(2t_{a1}\right)^2}\right)\left[\boldsymbol{\rho}_v\right]_{10\times 4}^T\left[\mathbf{H}_{cc,1}\right]_{4\times 4}\left[\boldsymbol{\rho}_v\right]_{4\times 10},\\
&\left[\mathbf{k}_5\right]=\left(G_sh_wt_w+\frac{G_{a1}A_{a1}h_b^2}{t_{a1}^{\,2}}\right)\left[\boldsymbol{\rho}_{\theta x}\right]_{10\times 2}^T\left[\mathbf{H}_{ll}\right]_{2\times 2}\left[\boldsymbol{\rho}_{\theta x}\right]_{2\times 10},\\
&\left[\mathbf{k}_6\right]=\left[-G_sh_wt_w+G_{a1}A_{a1}\frac{\left(2t_{a1}+t_f+t_{g1}\right)h_b}{4t_{a1}^{\,2}}\right]\left(\left[\boldsymbol{\rho}_v\right]_{10\times 4}^T\left[\mathbf{H}_{cl,1o}\right]_{4\times 2}\left[\boldsymbol{\rho}_{\theta x}\right]_{2\times 10}+\left[\boldsymbol{\rho}_{\theta x}\right]_{10\times 2}^T\left[\mathbf{H}_{lc,o1}\right]_{2\times 4}\left[\boldsymbol{\rho}_v\right]_{4\times 10}\right),\\
&\left[\mathbf{k}_7\right]=+\bar{A}_{g1,11}b\left[\boldsymbol{\rho}_{w1}\right]_{10\times 2}^T\left[\mathbf{H}_{ll,1}\right]_{2\times 2}\left[\boldsymbol{\rho}_{w1}\right]_{2\times 10}, \qquad \left[\mathbf{k}_8\right]=\left(\frac{G_{a1}A_{a1}}{t_{a1}^{\,2}}\right)\left[\boldsymbol{\rho}_w\right]_{10\times 2}^T\left[\mathbf{H}_{ll}\right]_{2\times 2}\left[\boldsymbol{\rho}_w\right]_{2\times 10},\\
&\left[\mathbf{k}_9\right]=+\frac{1}{2}\left(G_{a1}A_{a1}\frac{\left(2t_{a1}+t_f+t_{g1}\right)}{t_{a1}^{\,2}}\right)\left(\left[\boldsymbol{\rho}_v\right]_{10\times 4}^T\left[\mathbf{H}_{cl,1o}\right]_{4\times 2}\left[\boldsymbol{\rho}_w\right]_{2\times 12}+\left[\boldsymbol{\rho}_w\right]_{12\times 2}^T\left[\mathbf{H}_{lc,o1}\right]_{2\times 4}\left[\boldsymbol{\rho}_v\right]_{4\times 10}\right),\\
&\left[\mathbf{k}_{10}\right]=\frac{1}{2}\left(\frac{G_{a1}A_{a1}h_b}{t_{a1}^{\,2}}\right)\left(\left[\boldsymbol{\rho}_w\right]_{10\times 2}^T\left[\mathbf{H}_{ll}\right]_{2\times 2}\left[\boldsymbol{\rho}_{\theta x}\right]_{2\times 10}+\left[\boldsymbol{\rho}_{\theta x}\right]_{10\times 2}^T\left[\mathbf{H}_{ll}\right]_{2\times 2}\left[\boldsymbol{\rho}_w\right]_{2\times 10}\right),\\
&\left[\mathbf{k}_{11}\right]=+G_{a1}A_{a1}\left(\frac{1}{t_{a1}}\right)^2\left[\boldsymbol{\rho}_{w1}\right]_{10\times 2}^T\left[\mathbf{H}_{ll}\right]_{2\times 2}\left[\boldsymbol{\rho}_{w1}\right]_{2\times 10},\\
&\left[\mathbf{k}_{12}\right]=-G_{a1}A_{a1}\left(\frac{1}{t_{a1}}\right)^2\left(\left[\boldsymbol{\rho}_w\right]_{10\times 2}^T\left[\mathbf{H}_{ll}\right]_{2\times 2}\left[\boldsymbol{\rho}_{w1}\right]_{2\times 10}+\left[\boldsymbol{\rho}_{w1}\right]_{10\times 2}^T\left[\mathbf{H}_{ll}\right]_{2\times 2}\left[\boldsymbol{\rho}_w\right]_{2\times 10}\right),\\
&\left[\mathbf{k}_{13}\right]=-G_{a1}A_{a1}\frac{1}{t_{a1}}\frac{\left(2t_{a1}+t_f+t_{g1}\right)}{2t_{a1}}\left(\left[\boldsymbol{\rho}_{w1}\right]_{10\times 2}^T\left[\mathbf{H}_{lc,o1}\right]_{2\times 4}\left[\boldsymbol{\rho}_v\right]_{4\times 10}+\left[\boldsymbol{\rho}_v\right]_{10\times 4}^T\left[\mathbf{H}_{cl,1o}\right]_{4\times 2}\left[\boldsymbol{\rho}_{w1}\right]_{2\times 10}\right),\\
&\left[\mathbf{k}_{14}\right]=-\frac{G_{a1}A_{a1}}{t_{a1}}\frac{h_b}{2t_{a1}}\left(\left[\boldsymbol{\rho}_{w1}\right]_{10\times 2}^T\left[\mathbf{H}_{ll}\right]_{2\times 2}\left[\boldsymbol{\rho}_{\theta x}\right]_{2\times 10}+\left[\boldsymbol{\rho}_{\theta x}\right]_{10\times 2}^T\left[\mathbf{H}_{ll}\right]_{2\times 2}\left[\boldsymbol{\rho}_{w1}\right]_{2\times 10}\right)
\end{aligned} \tag{2.1.3}$$

A2. 2 A steel beam element strengthened with a GFRP laminate bonded to the bottom flange (Eq. (40))

The governing displacement fields are interpolated from the nodal displacements as follows.

$$W(z)=\left\langle \mathbf{F}_l(z)\right\rangle_{1\times 2}^T\left[\boldsymbol{\rho}_w\right]_{2\times 10}\{\boldsymbol{\Delta}\}_{10\times 1},\qquad W_2(z)=\left\langle \mathbf{F}_l(z)\right\rangle_{1\times 2}^T\left[\boldsymbol{\rho}_{w2}\right]_{2\times 10}\{\boldsymbol{\Delta}\}_{10\times 1},$$
$$V(z)=\left\langle \mathbf{F}_c(z)\right\rangle_{1\times 4}^T\left[\boldsymbol{\rho}_v\right]_{4\times 10}\{\boldsymbol{\Delta}\}_{10\times 1},\qquad \theta_x(z)=\left\langle \mathbf{F}_l(z)\right\rangle_{1\times 2}^T\{\boldsymbol{\Delta}\}_{10\times 1} \tag{2.2.1}$$

in which the index matrices are defined as

$$\left[\boldsymbol{\rho}_w\right]_{2\times 10}=\left[\begin{array}{ccccc|ccccc}1&0&0&0&0&0&0&0&0&0\\0&0&0&0&0&1&0&0&0&0\end{array}\right],\quad \left[\boldsymbol{\rho}_{w2}\right]_{2\times 10}=\left[\begin{array}{ccccc|ccccc}0&1&0&0&0&0&0&0&0&0\\0&0&0&0&0&0&1&0&0&0\end{array}\right]$$
$$\left[\boldsymbol{\rho}_v\right]_{4\times 10}=\left[\begin{array}{ccccc|ccccc}0&0&1&0&0&0&0&0&0&0\\0&0&0&1&0&0&0&0&0&0\\0&0&0&0&0&0&0&1&0&0\\0&0&0&0&0&0&0&0&1&0\end{array}\right],\quad \left[\boldsymbol{\rho}_{\theta x}\right]_{2\times 10}=\left[\begin{array}{ccccc|ccccc}0&0&0&0&1&0&0&0&0&0\\0&0&0&0&0&0&0&0&0&1\end{array}\right] \tag{2.2.2}$$

and $\left\langle \mathbf{F}_l(z)\right\rangle_{1\times 2}^T,\left\langle \mathbf{F}_c(z)\right\rangle_{1\times 4}^T$ have been defined in Eq. (29). The component stiffnesses $\left[\mathbf{k}_i\right]_{12\times 12}$, $i=1,2,...,14$, defined in Eq. (40) can be determined as

$$\left[\mathbf{k}_1\right]=E_sA_s\left[\boldsymbol{\rho}_w\right]_{10\times 2}^T\left[\mathbf{H}_{ll,1}\right]_{2\times 2}\left[\boldsymbol{\rho}_w\right]_{2\times 10},\qquad \left[\mathbf{k}_2\right]=E_s\left(\frac{bt_fh_b^2}{2}+\frac{t_wh_b^3}{12}\right)\left[\boldsymbol{\rho}_{\theta x}\right]_{10\times 2}^T\left[\mathbf{H}_{ll,1}\right]_{2\times 2}\left[\boldsymbol{\rho}_{\theta x}\right]_{2\times 10},$$
$$\left[\mathbf{k}_3\right]=\left(E_s\frac{2bt_f^3}{12}+\bar{D}_{g2,11}b\right)\left[\boldsymbol{\rho}_v\right]_{10\times 4}^T\left[\mathbf{H}_{cc,2}\right]_{4\times 4}\left[\boldsymbol{\rho}_v\right]_{4\times 10},$$
$$\left[\mathbf{k}_4\right]=\left(G_sh_wt_w+G_{a2}A_{a2}\frac{\left(2t_{a2}+t_f+t_{g2}\right)^2}{\left(2t_{a2}\right)^2}\right)\left[\boldsymbol{\rho}_v\right]_{10\times 4}^T\left[\mathbf{H}_{cc,1}\right]_{4\times 4}\left[\boldsymbol{\rho}_v\right]_{4\times 10},$$
$$\left[\mathbf{k}_5\right]=\left(G_sh_wt_w+\frac{G_{a2}A_{a2}h_b^2}{{t_{a2}}^2}\right)\left[\boldsymbol{\rho}_{\theta x}\right]_{10\times 2}^T\left[\mathbf{H}_{ll}\right]_{2\times 2}\left[\boldsymbol{\rho}_{\theta x}\right]_{2\times 10},$$
$$\left[\mathbf{k}_6\right]=\left[-G_sh_wt_w+G_{a2}A_{a2}\frac{\left(2t_{a2}+t_f+t_{g2}\right)h_b}{4{t_{a2}}^2}\right]\left(\left[\boldsymbol{\rho}_v\right]_{10\times 4}^T\left[\mathbf{H}_{cl,1o}\right]_{4\times 2}\left[\boldsymbol{\rho}_{\theta x}\right]_{2\times 10}+\left[\boldsymbol{\rho}_{\theta x}\right]_{10\times 2}^T\left[\mathbf{H}_{lc,o1}\right]_{2\times 4}\left[\boldsymbol{\rho}_v\right]_{4\times 10}\right),$$
$$\left[\mathbf{k}_8\right]=\left(+\frac{G_{a2}A_{a2}}{{t_{a2}}^2}\right)\left[\boldsymbol{\rho}_w\right]_{10\times 2}^T\left[\mathbf{H}_{ll}\right]_{2\times 2}\left[\boldsymbol{\rho}_w\right]_{2\times 10},$$
$$\left[\mathbf{k}_9\right]=+\frac{1}{2}\left(-G_{a2}A_{a2}\frac{\left(2t_{a2}+t_f+t_{g2}\right)}{{t_{a2}}^2}\right)\left(\left[\boldsymbol{\rho}_v\right]_{10\times 4}^T\left[\mathbf{H}_{cl,1o}\right]_{4\times 2}\left[\boldsymbol{\rho}_w\right]_{2\times 10}+\left[\boldsymbol{\rho}_w\right]_{10\times 2}^T\left[\mathbf{H}_{lc,o1}\right]_{2\times 4}\left[\boldsymbol{\rho}_v\right]_{4\times 10}\right),$$
$$\left[\mathbf{k}_{10}\right]=\frac{1}{2}\left(-\frac{G_{a2}A_{a2}h_b}{{t_{a2}}^2}\right)\left(\left[\boldsymbol{\rho}_w\right]_{10\times 2}^T\left[\mathbf{H}_{ll}\right]_{2\times 2}\left[\boldsymbol{\rho}_{\theta x}\right]_{2\times 10}+\left[\boldsymbol{\rho}_{\theta x}\right]_{10\times 2}^T\left[\mathbf{H}_{ll}\right]_{2\times 2}\left[\boldsymbol{\rho}_w\right]_{2\times 10}\right),$$
$$\left[\mathbf{k}_{15}\right]=+\bar{A}_{g2,11}b\left[\boldsymbol{\rho}_{w2}\right]_{10\times 2}^T\left[\mathbf{H}_{ll,1}\right]_{2\times 2}\left[\boldsymbol{\rho}_{w2}\right]_{2\times 10},\quad \left[\mathbf{k}_{16}\right]=+G_{a2}A_{a2}\left(\frac{1}{t_{a2}}\right)^2\left[\boldsymbol{\rho}_{w2}\right]_{10\times 2}^T\left[\mathbf{H}_{ll}\right]_{2\times 2}\left[\boldsymbol{\rho}_{w2}\right]_{2\times 10},$$
$$\left[\mathbf{k}_{17}\right]=-G_{a2}A_{a2}\left(\frac{1}{t_{a2}}\right)^2\left(\left[\boldsymbol{\rho}_w\right]_{10\times 2}^T\left[\mathbf{H}_{ll}\right]_{2\times 2}\left[\boldsymbol{\rho}_{w2}\right]_{2\times 10}+\left[\boldsymbol{\rho}_{w2}\right]_{10\times 2}^T\left[\mathbf{H}_{ll}\right]_{2\times 2}\left[\boldsymbol{\rho}_w\right]_{2\times 10}\right),$$
$$\left[\mathbf{k}_{18}\right]=+\frac{G_{a2}A_{a2}}{t_{a2}}\frac{\left(2t_{a2}+t_f+t_{g2}\right)}{2t_{a2}}\left(\left[\boldsymbol{\rho}_{w2}\right]_{10\times 2}^T\left[\mathbf{H}_{lc,o1}\right]_{2\times 4}\left[\boldsymbol{\rho}_v\right]_{4\times 10}+\left[\boldsymbol{\rho}_v\right]_{10\times 4}^T\left[\mathbf{H}_{cl,1o}\right]_{4\times 2}\left[\boldsymbol{\rho}_{w2}\right]_{2\times 10}\right),$$
$$\left[\mathbf{k}_{19}\right]=+\frac{G_{a2}A_{a2}}{t_{a2}}\frac{h_b}{2t_{a2}}\left(\left[\boldsymbol{\rho}_{w2}\right]_{10\times 2}^T\left[\mathbf{H}_{ll}\right]_{2\times 2}\left[\boldsymbol{\rho}_{\theta x}\right]_{2\times 10}+\left[\boldsymbol{\rho}_{\theta x}\right]_{10\times 2}^T\left[\mathbf{H}_{ll}\right]_{2\times 2}\left[\boldsymbol{\rho}_{w2}\right]_{2\times 10}\right) \tag{2.2.3}$$

A2. 3 A steel beam element is not strengthened, as presented in Eqs. (42)

The governing displacement fields are interpolated from the nodal displacements as follows.

$$\begin{Bmatrix} W(z) \\ V(z) \\ \theta_x(z) \end{Bmatrix} = \begin{Bmatrix} \langle \mathbf{F}_l(z) \rangle_{1\times 2}^T [\boldsymbol{\rho}_w]_{2\times 8} \\ \langle \mathbf{F}_c(z) \rangle_{1\times 4}^T [\boldsymbol{\rho}_v]_{4\times 8} \\ \langle \mathbf{F}_l(z) \rangle_{1\times 2}^T [\boldsymbol{\rho}_{\theta x}]_{2\times 8} \end{Bmatrix} \{\boldsymbol{\Delta}\}_{8\times 1} \tag{2.3.1}$$

in which the index matrices are defined as

$$[\boldsymbol{\rho}_w]_{2\times 8} = \begin{bmatrix} 1 & 0 & 0 & 0 & 0 & 0 & 0 & 0 \\ 0 & 0 & 0 & 0 & 1 & 0 & 0 & 0 \end{bmatrix}, \quad [\boldsymbol{\rho}_v]_{4\times 8} = \begin{bmatrix} 0 & 1 & 0 & 0 & 0 & 0 & 0 & 0 \\ 0 & 0 & 1 & 0 & 0 & 0 & 0 & 0 \\ 0 & 0 & 0 & 0 & 0 & 1 & 0 & 0 \\ 0 & 0 & 0 & 0 & 0 & 0 & 1 & 0 \end{bmatrix},$$
$$[\boldsymbol{\rho}_{\theta x}]_{2\times 8} = \begin{bmatrix} 0 & 0 & 0 & 1 & 0 & 0 & 0 & 0 \\ 0 & 0 & 0 & 0 & 0 & 0 & 0 & 1 \end{bmatrix} \tag{2.3.2}$$

and $\langle \mathbf{F}_l(z) \rangle_{1\times 2}^T, \langle \mathbf{F}_c(z) \rangle_{1\times 4}^T$ have been defined in Eq. (29). The component stiffnesses $[\mathbf{k}_i]_{12\times 12}$, $i = 1,2,...,6$, defined in Eq. (42) can be determined as

$$[\mathbf{k}_1] = E_s A_s [\boldsymbol{\rho}_w]_{8\times 2}^T [\mathbf{H}_{ll,1}]_{2\times 2} [\boldsymbol{\rho}_w]_{2\times 8}, \quad [\mathbf{k}_2] = E_s \left(\frac{b t_f h_b^2}{2} + \frac{t_w h_b^3}{12} \right) [\boldsymbol{\rho}_{\theta x}]_{8\times 2}^T [\mathbf{H}_{ll,1}]_{2\times 2} [\boldsymbol{\rho}_{\theta x}]_{2\times 8},$$
$$[\mathbf{k}_3] = \left(E_s \frac{2 b t_f^3}{12} \right) [\boldsymbol{\rho}_v]_{8\times 4}^T [\mathbf{H}_{cc,2}]_{4\times 4} [\boldsymbol{\rho}_v]_{4\times 8}, \qquad [\mathbf{k}_4] = (t_w h_w) [\boldsymbol{\rho}_v]_{8\times 4}^T [\mathbf{H}_{cc,1}]_{4\times 4} [\boldsymbol{\rho}_v]_{4\times 8}, \tag{2.3.2}$$
$$[\mathbf{k}_5] = (t_w h_w) [\boldsymbol{\rho}_{\theta x}]_{8\times 2}^T [\mathbf{H}_{ll}]_{2\times 2} [\boldsymbol{\rho}_{\theta x}]_{2\times 8}, \qquad [\mathbf{k}_6] = [-t_w h_w] \left([\boldsymbol{\rho}_v]_{8\times 4}^T [\mathbf{H}_{cl,1o}]_{4\times 2} [\boldsymbol{\rho}_{\theta x}]_{2\times 8} + [\boldsymbol{\rho}_{\theta x}]_{8\times 2}^T [\mathbf{H}_{lc,o1}]_{2\times 4} [\boldsymbol{\rho}_v]_{4\times 8} \right)$$